

**Biogenic Gas Dynamics in Peat Soil Blocks using Ground Penetrating Radar: a
Comparative Study in the Laboratory between Peat Soils from the Everglades and
from two Northern Peatlands in Minnesota and Maine**

by

Anastasija Cabolova

A Thesis Submitted to the Faculty of
The Charles E. Schmidt College of Science
in Partial Fulfillment of the Requirements for the Degree of
Master of Science

Florida Atlantic University

Boca Raton, Florida

December 2010

Copyright by Anastasija Cabolova 2010

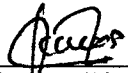
**Biogenic Gas Dynamics in Peat Soil Blocks using Ground Penetrating Radar: a
Comparative Study in the Laboratory between Peat Soils from the Everglades and
from two Northern Peatlands in Minnesota and Maine**

by

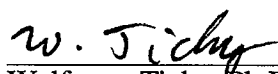
Anastasija Cabolova

This thesis was prepared under the direction of the candidate's thesis advisor, Dr. Xavier Comas, and co-advisor, Dr. Wolfgang Tichy, Department of Physics, and has been approved by the members of her supervisory committee. It was submitted to the faculty of the Charles E. Schmidt College of Science and was accepted in partial fulfillment of the requirements for the degree of Master of Science.

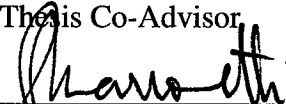
SUPERVISORY COMMITTEE:




Xavier Comas, Ph.D.
Thesis Advisor



Wolfgang Tichy, Ph.D.
Thesis Co-Advisor

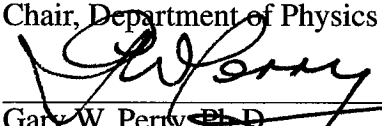


Pedro Marronetti, Ph.D.



Warner Miller, Ph.D.

Chair, Department of Physics



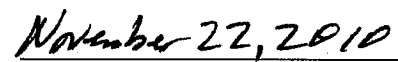
Gary W. Perry, Ph.D.

Dean, The Charles E. Schmidt College of Science



Barry T. Rosson, Ph.D.

Dean, Graduate College



Date

Acknowledgements

I would like to thank my advisor Dr. Xavier Comas, co-advisor Dr. Wolfgang Tichy, and Dr. Marronetti for the insightful reviews. Also thanks to Tyler Beck (Biology Dept., FAU) and Diego Quiros (Cornell University) for their help with sample collection and Mark Royer for his help with setup construction. In addition, thanks to Dr. Lee Slater (Rutgers University) for providing some of the equipment. Thanks as well to William Wright (FAU) for his help with data acquisition. Finally I thank the Environmental Sciences Program at FAU and the Everglades National Park for partial funding through an Environmental Sciences Everglades Internship.

Abstract

Author: Anastasija Cabolova

Title: Biogenic Gas Dynamics in Peat Soil Blocks using Ground Penetrating Radar:
a Comparative Study in the Laboratory between Peat Soils from the Everglades and two Northern Peatlands in Minnesota and Maine

Institution: Florida Atlantic University

Thesis Advisors: Dr. Xavier Comas
Dr. Wolfgang Tichy

Degree: Master of Science

Year: 2010

Peatlands cover a total area of approximately 3 million square kilometers and are one of the largest natural sources of atmospheric methane (CH_4) and carbon dioxide (CO_2). Most traditional methods used to estimate biogenic gas dynamics are invasive and provide little or no information about lateral distribution of gas. In contrast, Ground Penetrating Radar (GPR) is an emerging technique for non-invasive investigation of gas dynamics in peat soils. This thesis establishes a direct comparison between gas dynamics (i.e. build-up and release) of four different types of peat soil using GPR. Peat soil blocks were collected at peatlands with contrasting latitudes, including the Everglades, Maine and Minnesota. A unique two-antenna GPR setup was used to monitor biogenic gas buildup and ebullition events over a period of 4.5 months, constraining GPR data with surface deformation measurements and direct CH_4 and CO_2 concentration measurements. The effect of atmospheric pressure was also investigated. This study has implications for better understanding global gas dynamics and carbon cycling in peat soils and its role in climate change.

**Biogenic Gas Dynamics in Peat Soil Blocks using Ground Penetrating Radar: a
Comparative Study in the Laboratory between Peat Soils from the Everglades and
from two Northern Peatlands in Minnesota and Maine**

List of Tables.....	ix
List of Figures	xi
1 Introduction	1
1.1 Wetlands / Peatlands	1
1.2 Importance of Peatlands	2
1.2.1 Dynamics of gas release.....	3
1.2.2 Current models for gas storage and release in peatlands	4
1.3 Methodology used to investigate gas dynamics	4
1.4 Previous work with GPR.....	6
1.5 Thesis Objectives.....	6
2 Theoretical background	9
2.1 Ground Penetrating Radar	11
2.2 Gas content estimations.....	11
2.3 Additional Measurements.....	14
2.3.1 Gas Analyzer	14
2.3.2 Surface Deformation	16
2.3.3 Peat/water chemistry	16
2.3.4 Atmospheric Pressure	17
2.3.5 Porosity	18

3	Experimental Design	20
3.1	Field Sites	20
3.1.1	Everglades Wetland	20
3.1.2	Glacial Lake Agassiz Peatlands, Minnesota	21
3.1.3	Caribou Bog, Maine	22
3.2	Sample Extraction	22
3.3	Extracted Peat, Properties and Evaluation	23
3.3.1	Water Conservation Area 1 (WCA1)	24
3.3.2	Water Conservation Area 2 (WCA2)	25
3.3.3	<i>Sphagnum</i> , GLAP	25
3.3.4	<i>Sphagnum</i> , Maine	26
3.4	Laboratory Setup	26
3.4.1	Horizontal and Vertical Setups	27
3.5	Data acquisition modes	29
3.6	Ground Penetrating Radar Setup	31
3.6.1	Antennas	31
3.7	ProEx Control Unit	34
3.8	Laboratory Measurements	35
3.9	Data Processing	37
3.9.1	Filtering	37
3.9.2	Pickings	39
4	Results	40
4.1	Ground Penetrating Radar measurements	40
4.2	Ebullition events and surface deformation measurements	49
4.3	Gas meter measurements	61
4.4	Water chemistry analysis	67

4.5	Porosity Test.....	69
4.6	Exponential parameter comparison, WCA1	70
4.7	Error calculations	71
5	Discussion	76
5.1	Gas content and ebullition fluxes	76
5.2	Dynamics of ebullition.....	79
5.3	Effect of atmospheric pressure and correlation analysis	80
6	Future Work	87
7	Conclusions	91
8	Abbreviations	93
	Bibliography	94

List of Tables

3.1	Table: Characteristics of extracted peat samples	24
3.2	Dates of the experiment, 2010	35
4.1	WCA1 average, maximum gas content, maximum change and emission rate	42
4.2	WCA2 average, maximum gas content, maximum change and emission rate	44
4.3	<i>Sphagnum</i> , GLAP, average, maximum gas content, maximum change and emission rate	46
4.4	<i>Sphagnum</i> , Maine, average, maximum gas content, maximum change and emission rate	48
4.5	WCA1 dates and percentage of gas emissions, corresponding atmo- spheric pressure increase and surface deformation	55
4.6	WCA2 dates and percentage of gas emissions, corresponding atmo- spheric pressure increase and surface deformation	56
4.7	<i>Sphagnum</i> , GLAP dates and percentage of gas emissions, correspond- ing atmospheric pressure increase and surface deformation	56
4.8	<i>Sphagnum</i> , ME dates and percentage of gas emissions, corresponding atmospheric pressure increase and surface deformation	57
4.9	Gas flux rates estimated from GPR data per one ebullition event along with atmospheric pressure increase and surface deformation decrease for each peat sample (amount of gas is multiplied by three to approxi- mate gas ebullition from all three vertical lines)	59
4.10	Maximum CH_4 and CO_2 concentrations (% per vol) for all peat samples	67
4.11	Results of water analysis	67

4.12 Porosity Calculation: Total extracted volume and its mass, mass of dry peat and volume of water for each sample	69
4.13 Maximum change of gas content n for different parameters α	71
4.14 Measurements Variance for gas content error estimations	73
4.15 Measurements Variance for gas change error estimations.....	74
4.16 Total gas volume measurement error	75
4.17 Gas change measurement error	75
5.1 Gas Emissions per Surface Area and Average Rates of Methane and Carbon Dioxide Emission	78
5.2 Average CH_4 , CO_2 gas emissions of four single ebullition events per surface area per day for each sample.	78

List of Figures

2.1	Scheme of GPR connections (computer, unit and antennas)	11
2.2	Relative dielectric permittivity of water dependence on temperature for frequency range 0.2 - 8.9 GHz, [Buchner et al, 1999]	14
2.3	GEMTM2000 Gas Analyzer.....	15
2.4	Surface deformation measurement along Line B	16
2.5	Onset HOBO micro-station with pre-installed pressure and temperature smart sensors	18
3.1	Map of distinct peat extraction sites in Florida, Minnesota and Maine.....	21
3.2	Map of Everglades with Water Conservation Areas, Florida [Goldstein, 1994]	22
3.3	Extraction of <i>Sphagnum</i> peat block, Maine	23
3.4	Dimensions of the sample holder.....	27
3.5	(a)Vertical setup; (b) horizontal setup	28
3.6	Signal traveling path and time	29
3.7	Three types of geophysical GPR survey. Tx - Transmitter, Rx- receiver. Modified from Neal (2004)	29
3.8	Tomography setup. a) first file b) second file etc	30
3.9	Inner structure of GPR high-frequency shielded antenna [from MALA presentation in Charleston, SC]	31
3.10	WCA1, GPR signal	32
3.11	Container and line dimensions	36
3.12	WCA1 Line 1, picking of the "air" and "peat" signals	39

4.1	WCA1, gas content (GPR) for horizontal lines 1, 2 and 3, and their average gas content.....	41
4.2	WCA1, gas content (GPR) for vertical lines A, B and C, and their average gas content	42
4.3	WCA2, gas content (GPR) for horizontal lines 1, 2 and 3, and their average gas content.....	43
4.4	WCA2, gas content (GPR) for vertical lines A, B and C, and their average gas content	44
4.5	<i>Sphagnum</i> (GLAP), gas content (GPR) for horizontal lines 1, 2 and 3, and their average gas content	45
4.6	<i>Sphagnum</i> (GLAP), gas content (GPR) for vertical lines A, B and C, and their average gas content	46
4.7	<i>Sphagnum</i> (Maine), gas content (GPR) for horizontal lines 1, 2 and 3, and their average gas content	47
4.8	<i>Sphagnum</i> (Maine), gas content (GPR) for vertical lines A, B and C, and their average gas content	48
4.9	WCA1, Average Gas Content (GPR) for horizontal and vertical lines, Surface Deformation and Pressure (pressure axis is inverted), arrows indicating increase in atm. pressure match with gas content drops	50
4.10	WCA2, Average Gas Content (GPR) for horizontal and vertical lines, Surface Deformation and Pressure (pressure axis is inverted), arrows indicating increase in atm. pressure match with gas content drops	51
4.11	<i>Sphagnum</i> (GLAP), Average Gas Content (GPR) for horizontal and vertical lines, Surface Deformation and Pressure (pressure axis is inverted), arrows indicating increase in atm. pressure match with gas content drops	52

4.12	<i>Sphagnum</i> (Maine), Average Gas Content (GPR) for horizontal and vertical lines, Surface Deformation and Pressure (pressure axis is inverted), arrows indicating increase in atm. pressure match with gas content drops	53
4.13	Horizontal lines' Average GPR gas content: WCA1, WCA2, <i>Sphagnum</i> (GLAP), <i>Sphagnum</i> (Maine) and atmospheric pressure (axis inverted), arrows indicating increase in atm. pressure match with gas content drops	53
4.14	Vertical lines' Average GPR gas content: WCA1, WCA2, <i>Sphagnum</i> (GLAP), <i>Sphagnum</i> (Maine) and atmospheric pressure (axis inverted), arrows indicating increase in atm. pressure match with gas content drops	54
4.15	WCA1 four major gas ebullition events (1st - green, 2nd - violet, 3rd - blue, 4th - yellow)	60
4.16	WCA2 four major gas ebullition events (1st - green, 2nd - violet, 3rd - blue, 4th - yellow)	60
4.17	<i>Sphagnum</i> , GLAP four major gas ebullition events (1st - green, 2nd - violet, 3rd - blue, 4th - yellow)	61
4.18	<i>Sphagnum</i> , Maine four major gas ebullition events (1st - green, 2nd - violet, 3rd - blue, 4th - yellow)	61
4.19	Gas Meter Measurements (average of two bulk concentrations (CH_4 and CO_2) measurements) and GPR Data, WCA1, arrows indicating dates of similar trends in GPR and gas meter measurements	63
4.20	Gas Meter Measurements (average of two bulk concentrations (CH_4 and CO_2) measurements) and GPR Data, WCA2, arrows indicating dates of similar trends in GPR and gas meter measurements	64
4.21	Gas Meter Measurements (average value of two measurements of bulk concentrations of CH_4 and CO_2) in comparison with GPR Data, <i>Sphagnum</i> (GLAP), arrows indicating dates of similar trends in GPR and gas meter measurements	65

4.22	Gas Meter Measurements (average value of two bulk concentrations measurements of CH_4 and CO_2) in comparison with GPR Data, <i>Sphagnum</i> (Maine), arrows indicating dates of similar trends in GPR and gas meter measurements	66
4.23	TDS and Conductivity measurements of WCA1 and <i>Sphagnum</i> (GLAP)	69
4.24	WCA1 gas content curves comparison depending on α	70
5.1	Atmospheric pressure change vs gas content change within WCA1 sample (dotted lines represent the best fit error)	81
5.2	Atmospheric pressure change vs gas content change within WCA2 sample (dotted lines represent the best fit error)	83
5.3	Atmospheric pressure change vs gas content change within <i>Sphagnum</i> , GLAP sample (dotted lines represent the best fit error)	84
5.4	Atmospheric pressure change vs gas content change within <i>Sphagnum</i> , ME sample (dotted lines represent the best fit error)	85
6.1	Tomography, WCA1, 2D velocity model	87
6.2	Original Tomography-Ray model (one ray represent EM signal traveling from Tx to Rx)	88
6.3	Two neighboring traces of Tomography profile.....	89
6.4	Final Tomography-Ray model	90

1 Introduction

1.1 Wetlands / Peatlands

Wetlands are complex ecological communities that together with their environments form a functioning whole in nature [Patten and Jorgensen, 1995]. Wetlands are considered to be three component ecosystems [Mitsch et al., 2009], that include specific hydrology, soil chemistry and vegetation community. In order for wetlands to form, the land has to be saturated with water long enough to promote wetland processes as indicated by poorly drained soils, hydrophytic vegetation and various kinds of biological activities, which are associated with wet environments [Tarnocai et al., 1988].

Wetlands are generally divided into three major groups:

- Coastal wetlands - salt marshes, tidal freshwater marshes, mangrove swamps
- Freshwater swamps and marshes
- Peatlands [Mitsch et al., 2009]

In terms of total area, wetlands cover $580 \cdot 10^6$ ha in the world with an estimated 60% total corresponding to peatlands [Mitsch et al., 2009]. Wetland distribution is roughly bimodal with approximately 50% located in boreal and arctic regions (e.g. 50 to 70N, dominated by boreal peatlands), and about 35% located in tropical/subtropical regions (between 20N to 30S, dominated by swamps and marshes) [Matthews, 2000]. Overall, wetlands release approximately 145 Tg of methane (CH_4) per year, which is about 25% of the total CH_4 emissions [Whalen, 2005]. Even though northern latitudes (arctic and boreal region)

provide the most suitable conditions for peat to form [Chadde, 1998], there are a number of vast peatlands in tropical, subtropical and temperate climates as well [Whalen, 2005], such as Everglades, FL. Florida's peat deposits are generally thought to be recent in age (approx. 7,000 years [Gleason et al., 1994]) and are dominated by organic deposits of varying thickness over sand, marl, limestone, or other material [Brown, 1992].

Peat soils are composed of dead remains of plants deposited under water-soaked conditions and are a result of incomplete decomposition [Chadde, 1998]. Peatlands are characterized by extreme environmental conditions (anaerobic, acidic and nutrient-poor) not found in other wetland ecosystems. In addition, they are exceptionally stable and can persist for centuries [Chadde, 1998] with vertical accumulation rates of 20 to 100 cm per 1,000 years for European bogs [Moore and Bellamy, 1974; Malmer, 1975] and 100 to 200 cm per 1,000 years for North American bogs [Cameron, 1970]. Such accumulation rates are determined by the rate of litter production and organic matter decomposition [Mitsch et al., 2009].

1.2 Importance of Peatlands

Peatlands are one of the largest natural sources of biogenic gas, including atmospheric methane (CH_4) [Coulthard et al., 2009] and carbon dioxide (CO_2), thus play critical role in the global carbon cycle. Compared to tropical and subtropical systems, northern peatlands are the vastest in terms of surface area, thus traditionally the most studied. Nonetheless, tropical peatlands store significant amounts of CH_4 and CO_2 [Martini et al., 2006; Richardson and Huvan, 2008].

Total carbon storage in peatlands is estimated between 270-370 Tg, amounting for approximately 35-50% of the total 796 Tg C held in the atmosphere as CO_2 [Turunen et al. 2002; IPCC 2007]. Tropical peatlands show the highest uncertainties from all the estimates, with carbon storages ranging between 8 to 258 Tg [Hooijer et al. 2006]. For these reasons, estimating of biogenic gas volume, storage and release mechanisms in equatorial latitudes proves critical to better understand C cycling and potentially incorporate results

into climate change models.

1.2.1 Dynamics of gas release

Biogenic gas generated in peat soils can be trapped inside the peat's matrix as bubbles and can affect not only soil hydrology [Parsekian et al., 2010; Coulthard et al., 2009] but physical and chemical properties as well, like bulk permittivity, conductivity, pH etc. Methanogenic *archaea* (bacteria-like microorganism) is responsible for methane production in subsurface anaerobic zone (catotelm), while methanotropic bacteria is responsible for oxidation of CH_4 to CO_2 in the upper aerobic zone (acrotelm) [Whalen, 2005].

Biogenic gas releases from peatlands occur through three different mechanisms:

- Diffusion
- Wicking through vascular plants
- Ebullition [Blodau, 2002]

Gas diffusion is slow, more or less continuous release of gas and is usually associated with shallow gas storage [Coulthard et al., 2009]. Wicking is similar to diffusion with the exception that biogenic gas travels through inner structure in roots of vegetation and is being released on the surface through plant shoots [Rosenberry et al., 2006]. Ebullition, on the other hand, is an episodic release of free-phase gas in the form of bubbles and is generally greater in volume than diffusive fluxes [Rosenberry et al., 2006]. Percentage of methane released into the atmosphere also depends on the position of the water table, as much of the methane can be oxidized above water in case of diffusion and slow ebullition [Rosenberry et al., 2006].

1.2.2 Current models for gas storage and release in peatlands

Two currently existing models of biogenic gas storage consider either deep or shallow gas accumulations in peat soils and although they produce different patterns of gas accumulations, are not self-excluding [Coulthard, 2009].

The “deep gas” accumulation model suggests that CH_4 -containing bubbles can form deep below peat surface creating vast gas storages at depth greater than 2 m, below confining layers of woody peat [Glaser et al., 2004]. This model also proposes very large rates of methane and carbon dioxide loss to the atmosphere in a matter of minutes or hours, being related to drops of atmospheric pressure as one of the triggering factors of ebullition events.

The “shallow gas” storage model implies that the biogenic gas is formed at less than 1 m depth and the total gas volume is distributed in form of smaller gas bubbles in the subsurface of peat [Coulthard et al., 2009]. The model suggests that in this case large volumes of gas can be stored in the upper parts of peat without the need for confining woody layers [Coulthard et al., 2009].

Several triggering factors for the gas ebullition events have been considered, including changing water table, rainfall, temperature change, increases of atmospheric pressures etc [Crill et al., 1988; Glaser et al., 2004; Moore et al, 1990; Rosenberry, 2006; Tokida et al., 2005; Whalen, 2005; Comas et al, 2005]. Emissions in peatlands are influenced by other environmental variables such as soil chemistry, substrate quality and plant community structure [Matthews, 2000; Whalen, 2005].

1.3 Methodology used to investigate gas dynamics

Several techniques have been used over the last two decades to estimate gas content in peat soils, and although most of them imply invasive methods, some non-invasive efforts have also been recently used to estimate biogenic gas dynamics in northern peatlands.

Invasive techniques include methodologies such as direct sampling and Time Domain

Reflectometry (TDR) [Kellner and Lundin, 2001; Holden, 1997], DNA extraction (*Archea* microorganism investigations, which requires peat sampling and is not considered direct measure of gas volume) [Galland, 2004; Hales et al., 1996], piezometer installation [Rosenberry, 2006; Romanowicz et al., 1995; Glaser et al. 2004] and resistivity measurements [Slater et al., 2007].

TDR involves the insertion of probes into the soil. This method allows determination of water content in the soil, which can be ultimately related to gas content [Kellner and Lundin, 2001; Holden, 1997]. DNA extractions requires peat and peat-water investigations in laboratory [Galland, 2004], therefore small samples of peat have to be extracted from a site using a coring device (specially designed tube several cm in diameter) [Hales et al., 1996]. Piezometer slugs are usually installed near specially designed wells and give an estimate of hydraulic conductivity that is later related to the gas content [Rosenberry, 2006]. Resistivity measurements require electrode installation and are sensitive to 2% moisture content change within peat [Slater et al., 2007]. These techniques can give very good estimations of the current state and volume of the gas peat has produced at a particular location (point measurements), however they imply insertion of probes or sampling of the soil, therefore alter the gas regime and cannot be used to investigate gas dynamics at large scales.

Ground Penetrating Radar profiling [Comas and Slater, 2007; Comas et al., 2007], gas flux chambers [Ineson et al., 1998; Pihlatie, 2010] and surface deformation measurements [Strack et al., 2005, Rosenberry et al., 2006] are considered to be non-invasive techniques.

Gas chambers measure the flux of emitted gas and are considered to be indirect measurements of the gas volumes, since no measures of the gas content within the peat matrix are recorded [Pihlatie, 2010]. Surface deformations can be measured with elevation rods or by Global Positioning System [Glaser et al, 2004] in the field [Price, 2003] and using smaller scale elevation rods in laboratory studies [Comas and Slater, 2007], however they cannot give information about distribution of gas within the peat matrix.

Ground Penetrating Radar (GPR) uses electromagnetic waves to investigate the inner structure of geological materials, hence can be applied to peat matrix exploration [Comas and Slater, 2009]. Previous studies have already demonstrated the ability of GPR to infer information about biogenic gas distribution and dynamics in peat soils (Chapter 1.4).

1.4 Previous work with GPR

Ground Penetrating Radar has a wide range of uses, such as geological subsurface imaging [Doolittle and Butnor, 2009], contaminant mapping [Redman, 2009], utility detection in the construction areas, archeology investigations of large burials [Conyers, 2010] etc. GPR has also been used in the field [Comas et al., 2005, 2007, 2008; Parsekian et al., 2010; Strack and Mierau, 2010] and in the laboratory studies [Comas and Slater, 2007] for biogenic gas volumetric estimations using petrophysical models, such as Complex Refractive Index Model (CRIM) and showed consistent results with other measurements, like gas flux and surface deformation.

When used in the field, GPR is usually constrained with surface deformation and/or gas flux measurements. In addition, the water table position has to be monitored in order to correct for the water content, since the difference in height of water can be in order of 1 m. Nevertheless, the GPR survey produces good gas dynamics and ebullition estimates over large peatland areas [Parsekian et al., 2010; Strack and Mierau, 2010].

1.5 Thesis Objectives

Using GPR to study gas content variability in peat blocks of known size and dimensions in the laboratory allows constraining conditions in a way not feasible during field-scale studies and gives us the advantage of accurately constraining the EM signal travel distances. For instance, water table elevation in all samples was maintained at a constant value, thus any change in signal's travel times through the peat sample is assumed to be caused exclu-

sively by changes within the sample's matrix. In other words, and as already demonstrated in previous studies [i.e. Comas and Slater, 2007], we base our measurements on the fact that EM wave requires less time to travel from the transmitter to the receiver if transverse peat containing gas bubbles rather than water alone due to the contrasting relative permittivity values of air versus water. As a result, monitoring the time difference can give us information about variability of gas/water content at the pore-scale. Even though laboratory experiments do not necessarily provide a quantitative analysis of the gas content at the field site, it may help us to understand gas storage patterns, ebullition triggering events, as well as provide useful information of the environmental variables likely responsible for biogenic gas dynamics, such as changes in atmospheric pressure.

Three distinct peat samples, two from Everglades and one *Sphagnum* sample from a boreal peatland in Minnesota, were chosen in this laboratory study. One additional *Sphagnum* sample from a boreal peatland Maine (ME), was added later in March. The first objective of this thesis was to establish a direct comparison between gas production mechanisms of different types of peat collected at peatlands with contrasting latitudes and kept at the same laboratory conditions.

The second unique component of this experiment relies on the modified setup for the GPR data collection. Instead of using a GPR setup with a single antenna serving as both transmitter and receiver (as used in previous studies, i.e. Comas and Slater, 2007), a unique two-antenna configuration was used. This configuration has several advantages. First of all, the method increases precision on the travel distance measurements of the EM wave, for which derived gas content estimates are also enhanced in precision. Secondly, having a separate transmitter and receiver allows for further expansion of survey geometries and include configurations where both antennas can move independently from one another. For all these reasons, the second objective of this thesis is to test the applicability and reliability of this new GPR two-antenna setup as applied to gas dynamic studies in peat soils.

Finally, in this thesis GPR data is constrained with non-invasive surface deformation

measurements (following the setup shown in [Comas and Slater, 2007]), direct gas volume and concentration measurements, water chemistry analysis and porosity measurements in order to estimate variability within gas content and dynamics of different types of peat. Biogenic gas release in peat soils are known to be influenced by several environmental parameters (such as soil chemistry or substrate quality), and/or changes in temperature, water table elevation and atmospheric pressure. The third objective of this thesis is then to investigate how certain physical and chemical properties may influence gas dynamics in peat soils, and how certain environmental variables (such as atmospheric pressure) may influence the gas buildup and release in peat from contrasting latitudes under controlled laboratory conditions.

2 Theoretical background

Ground Penetrating Radar (GPR) is a well established geophysical technique for surveying the inner structure of geological materials [Annan, 2009]. GPR is based on electromagnetic (EM) wave propagation velocity (v), which is dependent on the physical properties of the medium (i.e. angular frequency $\omega = 2\pi f$, relative dielectric permittivity, ϵ_r , relative magnetic susceptibility, μ_r , conductivity, σ). [Neal, 2004]. However, for nonmagnetic materials ($\mu_r = 1$), low conductivities and high frequencies ($f > f_t$ - Eq. 2.1, where f_t is transition frequency for simple materials [Annan, 2009]), the velocity of EM wave in a medium of relative permittivity ϵ_r can be estimated by equation 2.2.

$$f_t = \frac{\sigma}{1\pi\epsilon} \quad (2.1)$$

$$v \approx \frac{c}{\sqrt{\epsilon_r}} \quad (2.2)$$

where c is speed of light.

As the EM wave propagates through medium, its amplitude of electrical field decays exponentially (Eq. 2.3)

$$E = E_0 \cdot e^{-\alpha r} \quad (2.3)$$

where r is depth, E is strength of the field and α is attenuation coefficient.

Attenuation coefficient α depends on conductivity σ of the medium, signal velocity and magnetic properties and can be calculated using equation 2.4 [Neal, 2004]

$$\alpha = \frac{\sigma}{2} \cdot \sqrt{\frac{\mu}{\epsilon}} \quad (2.4)$$

Thus, we can see that mostly conductivity influences the attenuation coefficient and for nonmagnetic materials α is greater, as conductivity increases and/or permittivity of the medium decreases. Equation 2.4 can be simplified defining impedance Z , which is assumed to be constant for any material (Eq. 2.5) [Annan, 2009]:

$$Z = \sqrt{\frac{\mu}{\epsilon}} \quad (2.5)$$

with impedance of free space defined as 377Ω .

Furthermore, under the assumptions that μ_r and σ are approximately constant throughout the medium, we can calculate the reflection coefficient (R) as (Eq. 2.6) [Neal, 2004].

$$R = \left(\frac{\sqrt{\epsilon_{r2}} - \sqrt{\epsilon_{r1}}}{\sqrt{\epsilon_{r2}} + \sqrt{\epsilon_{r1}}} \right)^2 = \left(\frac{v_2^{-1} - v_1^{-1}}{v_2^{-1} + v_1^{-1}} \right)^2 \quad (2.6)$$

where ϵ_1 and v_1 represent relative dielectric permittivity and velocity of first medium, and ϵ_2 and v_2 are relative dielectric permittivity and velocity of the encountered layer.

R values lies in the range 0 and +1, where 0 corresponds to full transmission and +1 to full reflection. The relation between transmission (T) and reflection coefficients (R) for incident wave can be seen in Eq. 2.7.

$$T = 1 - R \quad (2.7)$$

Reflection and transmission of the signal are essential properties for subsurface investigations, as the GPR ray travels into the material part of it is reflected and registered at the surface and the other part is able to travel further allowing a possibility of reflection from deeper layers.

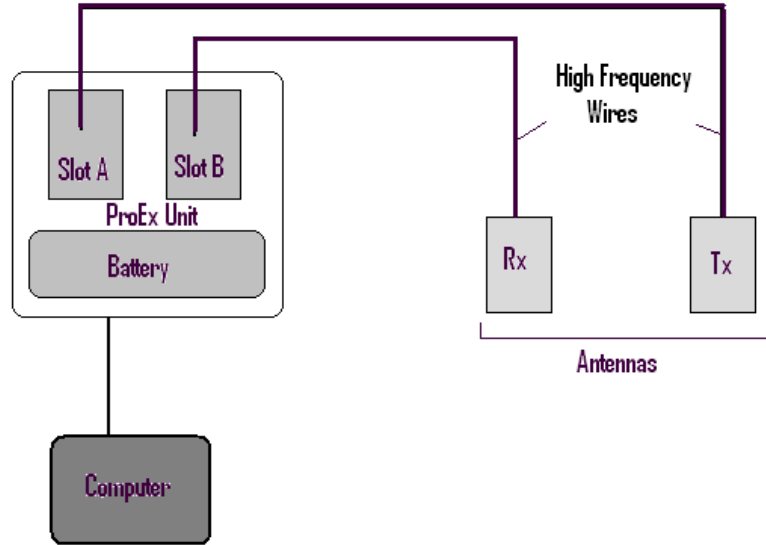


Figure 2.1: Scheme of GPR connections (computer, unit and antennas)

2.1 Ground Penetrating Radar

GPR consists of a transmitting and a receiving antennas and a control unit schematically shown in figure 2.1. When the EM wave encounters a contrast in relative dielectric permittivity (ϵ_r), the signal is reflected. As the receiving antenna records variations of the returned signal, the unit registers the time of the signal arrivals (commonly in nanoseconds, ns), allowing the computer to record the profile for later processing and analysis. Even though certain processing algorithms may result in loss of signal's true amplitude [Sandmeier, 1998], some processing steps are still necessary to perform in order to correctly interpret the behavior of the EM signal as it travels through geological materials. (More on Ground Penetrating Radar Setup in chapter 3.6)

2.2 Gas content estimations

One of the most commonly used equations to relate bulk relative dielectric permittivity to water content, θ , is the Topp equation (Eq. 2.8), which was established experimentally by

plotting known relative dielectric permittivity, ϵ_r , of a sample versus its water content, θ .

$$\theta = 4.3 \cdot 10^{-6} \epsilon_r^3 - 5.5 \cdot 10^{-4} \epsilon_r^2 + 2.92 \cdot 10^{-2} \epsilon_r - 5.3 \cdot 10^{-2} \quad (2.8)$$

However, Topp equation: (a) diverges for $\theta < 50\%$ (i.e. low values of relative permittivity, ϵ_r), (b) does not account for porosity, and (c) does not produce realistic results for soils with high organic content. For all these reasons Topp's equation is unsuitable for peat soils, which are considered to be $\approx 85\%$ organic matter [Mitsch et al., 2009].

Many attempts have been made to find dielectric permittivity of a mixture provided the permittivity of its components [Bottcher, 1952; Looyenga, 1965; Iglesias and Fernandez, 2001]. The most frequently used model is Looyenga's equation (Eq. 2.9 [Looyenga, 1965; Nelson, 2001]) for particles of all shapes that can be modified for two-phase and three-phase mixtures.

$$\epsilon^{1/3} = v_1 \epsilon_1^{1/3} + v_2 \epsilon_2^{1/3} + v_3 \epsilon_3^{1/3} \quad (2.9)$$

where v_1 , v_2 and v_3 are fractional volumes and their sum has to be equal to 1 (Eq. 2.10)

$$v_1 + v_2 + v_3 = 1 \quad (2.10)$$

The Complex Refractive Index Model (CRIM) is very similar to Looyenga's equation with: (a) defined and simplified with the help of equation 2.10 fractional volumes (b) instead of fixed exponent $\frac{1}{3}$, the fitting parameter α depends on orientation of mixture's components and ranges from -1 to +1 (Eq. 2.11):

$$\epsilon_b^\alpha = \theta \epsilon_w^\alpha + (1 - \phi) \epsilon_s^\alpha + (\phi - \theta) \epsilon_a^\alpha \quad (2.11)$$

where ϕ is soil porosity (see section 2.3.5), θ is moisture content (ratio of total volume of water to total volume of the investigated medium), ϵ_b is bulk dielectric permittivity and ϵ_w ,

ϵ_s and ϵ_a are water, soil and air permittivities respectively. Note, that permittivity of air, ϵ_0 , can be factored out and permittivities replaced by relative values.

Solving the equation 2.11 for gas content, $n = \phi - \theta$, we can estimate the fractional volume of the stored gas (Eq. 2.12):

$$n = \frac{\phi\epsilon_w^\alpha + (1 - \phi)\epsilon_s^\alpha - \epsilon_b^\alpha}{\epsilon_w^\alpha - \epsilon_a^\alpha} \quad (2.12)$$

where ϕ has to be determined using equation 2.16 as later explained (see section 2.3.5).

Several studies [i.e. Brovelli et al, 2008] have investigated the most appropriate values for parameter α according to soil type. Values $\alpha = 0.35$ are well accepted for organic porous matter [Kellner et al, 2005] which is close to the Looyenga's equation $\alpha = 1/3$, $\alpha = 1/2$, generally used for most materials [Brovelli et. al., 2008] and $\alpha = 0.04\phi + 0.47$ for water saturated two-phase mixtures [Brovelli et. al 2008].

The soil (in our case, peat) relative permittivity ϵ_s had to be estimated in a range between 1.5 and 7.5 [Ayalew et al., 2007]. For all samples the values relative dielectric permittivity of soil, ϵ_{rs} , was chosen to be between 2 and 4 [Comas and Slater, 2007; Kellner and Lundin, 2001; Alayew, 2007]. Even though the total gas content in the sample is affected by the numerical choice in relative permittivity of the soil, relative changes in gas content are barely affected by such small variability (i.e. 2-4).

Relative dielectric permittivity of water ϵ_w depends on temperature [Buchner et al, 1999]. Buchner determined complex dielectric permittivity of water by means of two waveguide interferometers in the 0.2 GHz and 89 GHz frequency range for temperatures ranging from 0° C to 35 ° C. The results and linear approximation are shown in figure 2.2.

Thus, knowing the temperature of peat-water, we can correct the relative dielectric permittivity of water using equation 2.13.

$$\epsilon_w = -0.3697 \cdot T + 87.669 \quad (2.13)$$

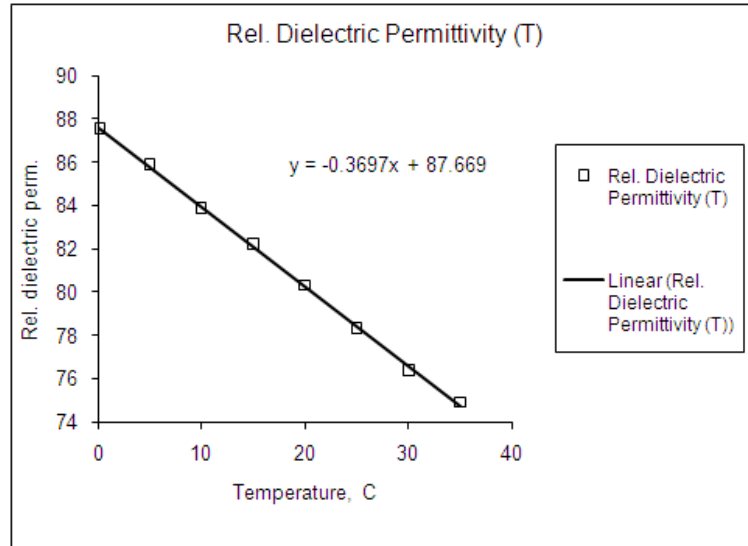


Figure 2.2: Relative dielectric permittivity of water dependence on temperature for frequency range 0.2 - 8.9 GHz, [Buchner et al, 1999]

Note, that even though the relative permittivity of peat was not measured in this experiment, it still remains constant and generally considered to be constant in time, thus does not affect the changes of gas content. In contrast, the changes in temperature do affect the relative permittivity of water from one day to another, therefore if not accounted, may result in poorly estimated gas content changes.

2.3 Additional Measurements

2.3.1 Gas Analyzer

In order to directly measure production of biogenic gas within the peat blocks and to constrain our GPR results the GEMTM2000 gas analyzer was used during four weeks to measure gas concentrations. For each concentration measurement the gas bubbles were extracted from the peat samples by means of syringe with 25 cm long blunt-pointed needle and then injected into the sample tube connected to the inlet port of the GEMTM2000 (Figure 2.3)

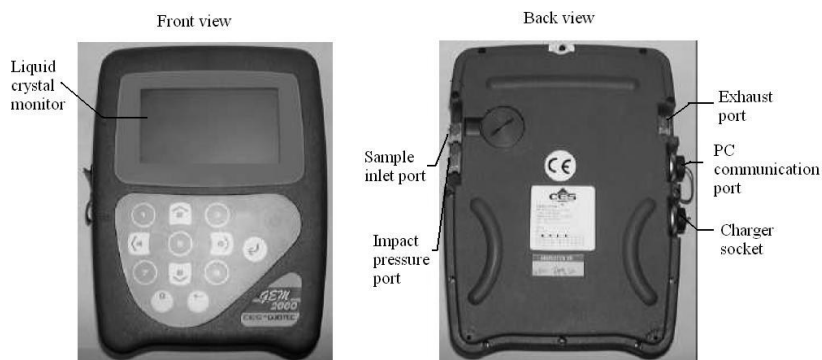


Figure 2.3: GEMTM2000 Gas Analyzer

The GEMTM2000 is designed by CES-LANDTEC specifically for use on landfills to monitor landfill gas (LFG). The GEMTM2000 analyses the methane (CH_4), carbon dioxide (CO_2) and oxygen (O_2) content. The percentage of input gas is displayed on liquid crystal monitor and can be either stored in the instrument or read directly from display [Landtec, 2005].

When switched on, the analyzer pumps in the air through protective filter into the sample inlet and measures concentrations of pre-installed gasses. The instrument is calibrated using certified methane mixtures (50% LEL, 2.5% vol in our case) and provides accurate readings, assuming no other hydrocarbon gasses are present within the sample (e.g. ethane, propane, butane, etc.). If other hydrocarbon are present, the methane reading will be higher (never lower) than the actual methane concentration being monitored [Landtec, 2005]. Other gasses found in peatlands sites will generally not affect the methane and the carbon dioxide readings [Landtec, 2005].

2.3.2 Surface Deformation

Surface deformation of a total of three lines (A, B and C) across the surface of each peat sample was measured before GPR data collection, as in [Comas and Slater, 2007]. Each line contained a total of five measurements performed with a small cylindrical ruler placed through specifically made holes in a wooden container cover (Fig. 2.4). For each surface deformation measurement the cover is placed on the sample holder in such a way that the ruler estimates the distance between the surface of the cover and exactly the same point on the surface of the peat each time. The thickness of the cover is then accounted and any deviation of the determined distance is assumed to be associated with the peat surface uplift or compression due to gas accumulation or release [Price, 2003; Slater et al., 2007; Comas and Slater, 2007].

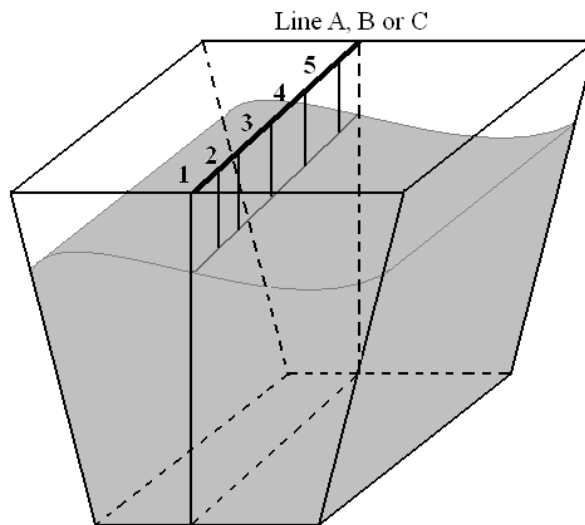


Figure 2.4: Surface deformation measurement along Line B

2.3.3 Peat/water chemistry

A fisher Scientific accumet AP85 Portable Waterproof pH/Conductivity Meter was used to measure water chemistry throughout the entire length of the experiment and after each

GPR measurement. Peat-water temperature, T , conductivity, σ , Total Dissolved Solids (TDS) and pH were measured by placing the conductivity and pH probes approximately 5 cm below the water table. After the conductivity was measured, water with the same conductivity was added (due to water evaporation, the samples had to be watered regularly). Measurements of water temperature were performed to account for changes in relative dielectric permittivity. Total dissolved solids measurements are the characteristics of non-organic materials present in the peat sample, which can be a measure of pollutants, and pH measurements were performed as it is regarded as one of the factors of biogenic gas production [Williams and Crawford, 1984]

2.3.4 Atmospheric Pressure

Atmospheric pressure and air temperature data was collected in the laboratory using a On-set HOBO micro-station data logger with pressure and temperature sensors (Fig. 2.5). Since changing atmospheric pressure is thought to be one of the triggering processes during gas ebullition events [Comas and Slater, 2007; Tokida et al., 2007], data points were continuously collected at 15 minute intervals over the whole duration of the experiment. The pressure and temperature measurements are automatically stored in the logger and are later downloaded to a computer for data processing.

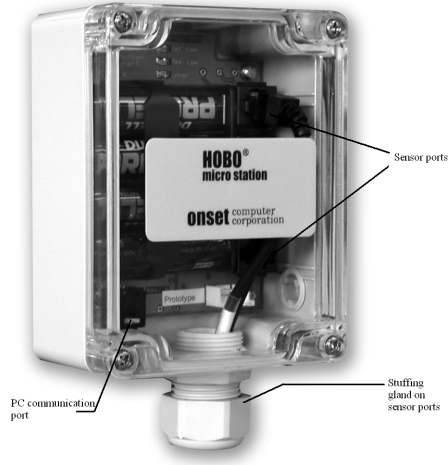


Figure 2.5: Onset HOBO micro-station with pre-installed pressure and temperature smart sensors

2.3.5 Porosity

Porosity is usually expressed as a percentage and can be defined as the ratio between the total volume of voids and the total volume of the porous medium (U.S. Geological Survey) (Eq. 2.14).

$$\phi = \frac{V_{space}}{V_{TOTAL}} = \frac{V_{TOTAL} - V_{material}}{V_{TOTAL}} \quad (2.14)$$

Assuming that the material (peat soil in our case) is fully saturated with water the equation 2.15 has to hold:

$$V_{TOTAL} = V_{material} + V_{water} \quad (2.15)$$

Solving equation 2.15 for the $V_{material}$ and plugging in the equation 2.14, we have the final equation for the porosity (Eq. 2.16)

$$\phi = \frac{V_{TOTAL} - V_{TOTAL} + V_{water}}{V_{TOTAL}} = \frac{V_{water}}{V_{TOTAL}} \quad (2.16)$$

Porosity measurements were performed following [ASABE Standards, 2008] and by: (1) extracting and weighting a known volume of fully water-saturated peat soils; (2) oven drying the volume at 103° C for 24 hours; and (3) re-weighting the sample and estimating the weight difference between the wet and dry sample to apply equation 2.16.

3 Experimental Design

3.1 Field Sites

Peat samples were extracted at four locations: Water Conservation Areas (WCA) 1 and 2, in the Florida Everglades, Caribou Bog, in Maine and Glacial Lake Agassiz Peatland (GLAP) in Minnesota (Figure 3.1). Following the objectives of this thesis as previously described in chapter 1.5, samples from contrasting latitudes were collected to establish a direct comparison between gas production mechanisms of different types of peat kept at the same laboratory conditions. All peat blocks were extracted from the surface of each peatland to investigate the dynamics of biogenic gases when considering a shallow gas accumulation model (see chapter 1.2.2). The first two sites correspond to Everglades and Loxahatchee peat and are representative of a large subtropical peatland, while the other two correspond to *Sphagnum* peat and are representative of northern peatlands in the boreal region. Each field site has distinct characteristics as described in the following sections.

3.1.1 Everglades Wetland

The Everglades is a relatively young subtropical wetland (only approximately 7,000 years old) and it stretches out for 700,000 ha [Gleason et. al., 1994]. It encompasses five Water Conservation Areas (WCAs) and is considered to be one of the largest wetland ecosystems in the world. The two vastest types of peatlands are Everglades and Loxahatchee (WCA1 and 2) [Craft and Richardson, 2008] (Figure 3.2 [Goldstein, 1994]). Peat thickness in the Everglades can reach up to 4 meters [Craft and Richardson, 2008] and should not be

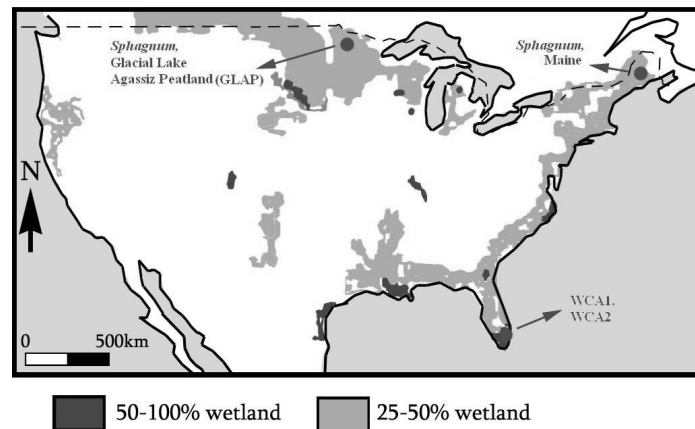


Figure 3.1: Map of distinct peat extraction sites in Florida, Minnesota and Maine

mistaken with a marsh or a swamp [Richardson and Huvan, 2008] due to the fact that peat forms by means of organic matter decomposition, whereas marshes and swamps are characterized exclusively by slow-moving waters and low topographic relief.

Everglades peat form a layer of 0.5 - 2 meters and is originated from Sawgrass (*Cladium jamaicense*), whereas the Loxahatchee peat is generally 1 - 3 meters thick and is thought to be derived from Water lily (*Nymphaea odorata*) [Craft and Richardson, 2008]. In addition, different densities of peat are characteristic for different areas of Everglades but usually range between 0.06 to 0.1 g/cm^3 for WCA1 and 2 [Craft and Richardson, 2008].

3.1.2 Glacial Lake Agassiz Peatlands, Minnesota

Glacial Lake Agassiz Peatlands (GLAP) are generally characterized by spruce forest, the presence of three-seeded sedge, *Carex Trisperma*, and lingoberry, *Vaccinium vitisidaea*, and the lack of fen indicator species [Parsekian et.al., 2010]. The formation of GLAP peat began approximately 12,000 years ago, making it almost twice as old as the Everglades peatland [Boelter, 1968]. Nevertheless, *Sphagnum* peats are thought to be less dense, with an average density of 0.02 g/cm^3 and less decomposed than Everglades peat [Boelter,

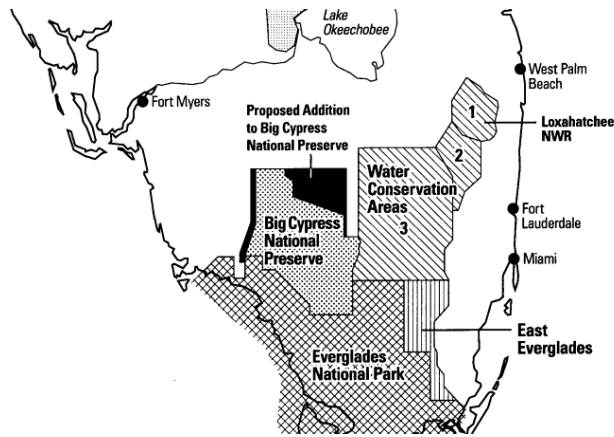


Figure 3.2: Map of Everglades with Water Conservation Areas, Florida [Goldstein, 1994]

1968]

3.1.3 Caribou Bog, Maine

Caribou Bog Peatland is approximately 10,000 - 10,500 years old [Hu and Davis, 1995]. It covers 2,200 ha near Bangor, Maine and is underlain by a mineral glacio-marine silt-clay [Osberg et al., 1985]. The field site, where the sample was extracted, lays in the Center Unit of the bog with two main plant communities distinguished: bryophytes and vascular plants [Comas et al., 2004]. The peatland is divided in large wooded heath areas, surrounded by *Sphagnum* lawn, low shrub areas and other smaller communities like fen, forested bogs and swamps [Davis and Anderson, 1999].

3.2 Sample Extraction

The same routine was followed for extraction of all samples in the field as described in Comas and Slater (2007), with all extracted samples being approximately 20L in volume. Briefly, peat blocks were extracted by cutting and pulling out the peat surrounding the block on the sides. The sample container was then placed on the top of the block and the base of the block was cut with a machete to complete removal (Fig. 3.3).



Figure 3.3: Extraction of *Sphagnum* peat block, Maine

After peat removal, the container was sealed and sent to the lab, where it would be either trimmed into a sample holder or put in the freezer until the experiment was ready to start. Freezing the peat does not destroy the methanogenic micro-organisms, but rather makes them inactive, imitating weather conditions in a landfill during the winter season [Mastepanov et al., 2008].

Although investigation of peat volumes from deeper areas may help better understanding biogenic gas dynamics for deeper soils (particularly for *Sphagnum* samples from thick northern peatlands), extraction of peat blocks with depth represents a series of challenges that were not feasible for the scope of this research.

3.3 Extracted Peat, Properties and Evaluation

Four different peat blocks were investigated in the experiment - two blocks correspond to Loxahatchee and Everglades peat soils from two distant areas of Everglades, and two

blocks correspond to *Sphagnum* Peat, one from Minnesota and the other from Maine. Below is the description of each type, the dates and the coordinates of the extraction plus an overall description based on a preliminary visual evaluation.

Table 3.1 shows conductivity, pH, TDS and temperature measurements for each sample taken either at the site during the extraction or after defrosting during the peat block mounting into the sample holder.

Location	Conductivity, $\mu S/m$	pH	TDS, ppm	Temperature, °C
WCA1	324	6.88	160.0	19.5
WCA2	536	6.26	266.0	24.6
<i>Sph</i> , GLAP	133	4.44	66.4	19.5
<i>Sph</i> , Maine	195.3	-	97.4	19.4

Table 3.1: Table: Characteristics of extracted peat samples

3.3.1 Water Conservation Area 1 (WCA1)

The peat block from Water Conservation Area 1 (UTM coordinates 17571009E 2939357N) was extracted from the surface in a freshwater marsh area next to a Sawgrass ridge. The sample was transported to the lab and kept frozen until the experiment was initiated on November, 9th. It was then gradually defrosted with progressive increments of 2-3 °C per day until room temperature was reached.

Decomposition level was estimated as H4-H5 (slightly decomposed) by the von Post Scale for assessing the degree of decomposition of peat [Ekono, 1981]. The surface of the sample was mostly peat moss, and limited amount of roots were found inside the peat block, when encasing the sample into the sample holder. The peat itself had a typical dark brown to black color and corresponds to Loxahatchee peat due to relatively high decomposition level and lack of roots [Craft and Richardson, 2008].

Characteristics of the peat sample after placement in the laboratory sample container

(on November 30th) were as follows: $pH = 6.88$, $\sigma_w = 324\mu S$; $TDS = 160ppm$ at temperature $T \approx 19.5^\circ C$ (Tab. 3.1). Level of pH higher than 4.8 indicates that this sample is of eutrophic peat type (nutrient rich tropical peatlands [Mitsch et al., 2009]) fens.

3.3.2 Water Conservation Area 2 (WCA2)

The soil sample extracted from WCA2 (UTM coordinates: 17566282E, 2900873N) was brown, showed presence of small roots and branches sized from half a centimeter to about 5 centimeters and most likely corresponds to Everglades peat [Craft and Richardson, 2008]. Decomposition was determined to be H3 or H4 (very slightly or slightly decomposed) by the von Post Scale for assessing the degree of decomposition of peat [Ekono, 1981]. The same parameters were measured in the field: $pH = 6.26$, $\sigma_w = 536\mu S$, $TDS = 266ppm$, $T = 24.6^\circ C$ (Tab. 3.1). Similarly to WCA1, this sample shows characteristics typical for eutrophic fens [Mitsch et al., 2009].

Water table in the field was about 70 cm below the surface, with the bedrock at approximately 1.40 - 1.80 cm from the surface of the peat. For that reason, the peat on the site was fairly dry. Even though the upper layer of peat usually remains intact, in this case it was necessary to cut approximately 2 cm from the top of the sample in order to properly fit it in the laboratory sample holder and to perform GPR vertical measurements as described later in the next section.

3.3.3 *Sphagnum*, GLAP

Similar to the sample from WCA1, the Glacial Lake Agassiz Peatland (GLAP) sample was kept frozen until the experiment was initiated on November, 9th and then gradually defrosted with 2-3 °C increment per day until room temperature was reached.

The *Sphagnum* peat sample was extracted from the very surface of the peatland. The sample was dark red to dark orange with vegetation (peat moss) in the upper surface and

presence of branches and roots. Decomposition was established as H3 level (very slightly decomposed) following the von Post scale [Ekono, 1981]. After placing the sample in the container it was saturated with water with a conductivity of $\sigma = 151\mu S/m$.

Characteristics of the peat sample after placement in the laboratory sample holder (on November 30th) were as follows: $pH = 4.44$, $\sigma_w = 133\mu S$; $TDS = 66.4ppm$ at temperature $T = 19.5^\circ C$ (Tab. 3.1).

3.3.4 *Sphagnum*, Maine

Measurements for this sample were initiated later, initiating gradual defrosting on the 17th of February with gradual temperature increases until almost reaching room temperature on March 9th. This is when the sample was cut and mounted into the container.

The level of sample decomposition was determined to be H2-H3 (almost undecomposed to slightly decomposed) by the von Post scale. The sample presented a red color characteristic of *Sphagnum* samples of Caribou Bog, and surface vegetation was kept intact. Characteristics of the peat sample after placement in the laboratory sample holder were as follows: $T = 14.9^\circ C$: conductivity $\sigma_w = 195.3\mu S$, $TDS = 97.4ppm$.

3.4 Laboratory Setup

In order to preserve the gas generating *Archea* (bacteria-like organism that produces biogenic gas) after sample extraction in the field, samples were frozen until ready to be measured. Peat blocks were gradually defrosted at about 2-3 degrees increase per day. Once defrosted, the samples were cut and fitted to 14.5 plastic sample holders. Caution was taken to disturb the peat matrix as little as possible during the sample mounting. Once the peat block was fitted in the holder and left for 48 hours (to allow the soil matrix to stabilize), measurements were initiated.

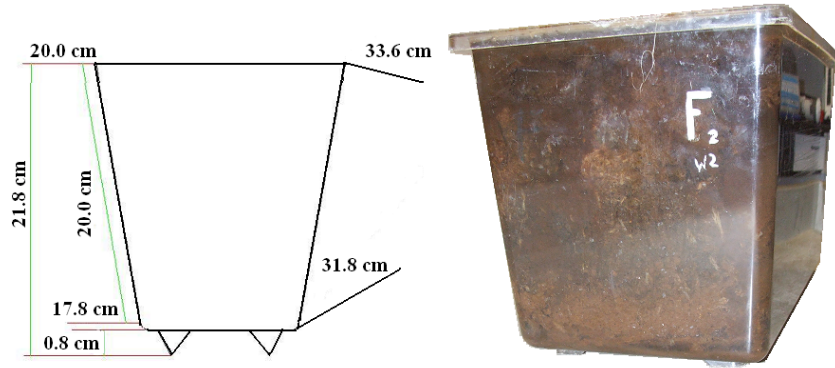


Figure 3.4: Dimensions of the sample holder

3.4.1 Horizontal and Vertical Setups

The laboratory setup was built entirely from wood to accommodate two 1.2 GHz shielded Ground Penetrating Radar (GPR) antennas and the sample holder for both horizontal and vertical line measurements (Figure 3.5). Wood was chosen to ensure that the signal was not being affected by induced EM currents when metallic parts are present. Following several improvements on an earlier version of the laboratory setup, both horizontal and vertical setups were modified in order for the peat block to remain stationary and the GPR antennas to move synchronically or independently (Chapter 3.5). The new setup prevented disturbance of peat matrix improving the quality of the measurements, while also allowing for GPR tomography, which requires independent shift of the antennas. For the vertical arrangement, line spacers were used to allow profile shifting horizontally without sample holder disturbance. This modification also decreased potential errors since we were able to add sample stoppers on the vertical sample holder and secure the same position of the container for all the measurements. In addition to that, vertical tomography could also be performed, which was not possible with the previous setup.

Horizontal antenna arrangement allows collection of 35 traces 1 cm apart per one data file. Each file is initiated and finished with a series of air measurements to correct for

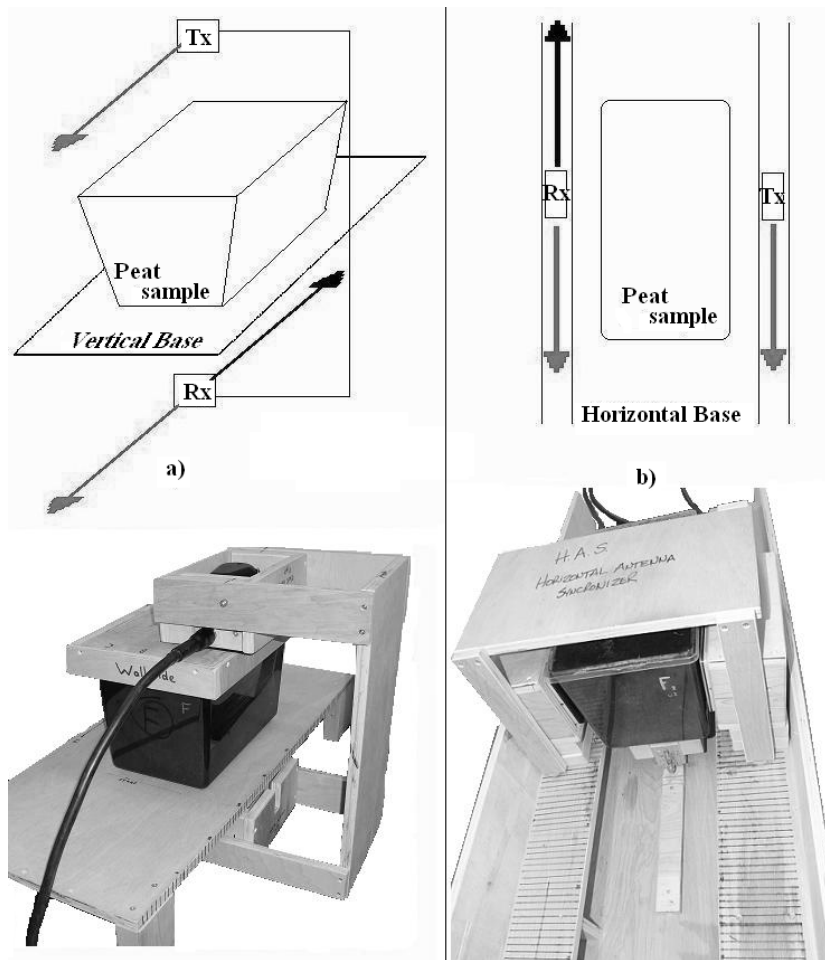


Figure 3.5: (a) Vertical setup; (b) horizontal setup

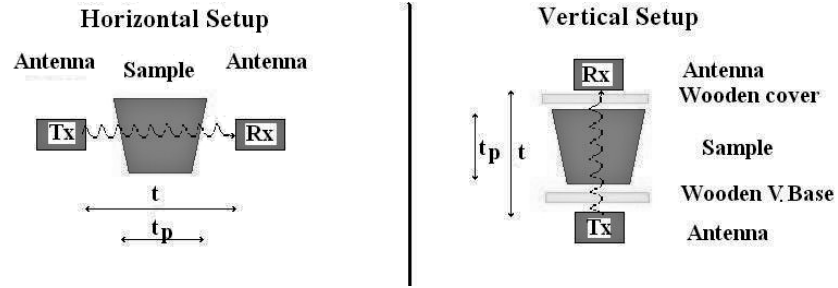


Figure 3.6: Signal traveling path and time

potential triggering time delays. This way, we are able to average the measured time it took for the signal to travel from one antenna to the other through air and subtract it from the measured time the pulse traveled through the sample (Figure 3.6). Triggering of the EM pulse was performed on keyboard mode to ensure high stacking (minimum of 64 stack or signal transmissions per trace) at intervals of 1 cm.

3.5 Data acquisition modes

A total of two different acquisition modes were used to collect data in this thesis, namely zero offset profiling (ZOP) and tomography (Figure 3.7)

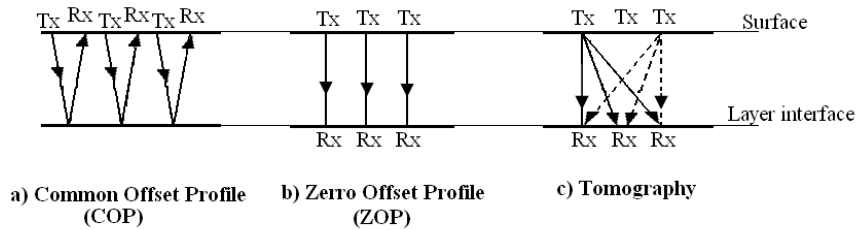


Figure 3.7: Three types of geophysical GPR survey. Tx - Transmitter, Rx- receiver. Modified from Neal (2004)

COP is arguably the most popular mode for GPR data acquisition. It requires the transmitter (Tx) and the receiver (Rx) to move with a constant separation between them while surveying (Figure 3.7), with the distance of separation dependent on the antennas' fre-

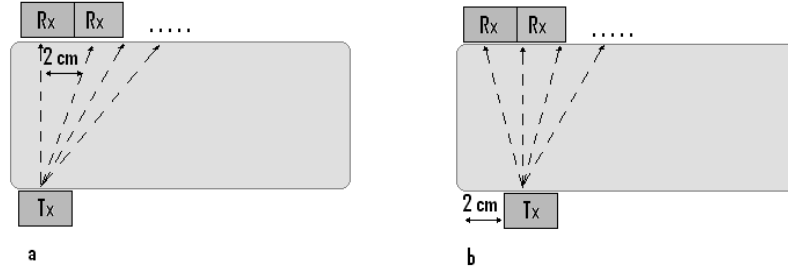


Figure 3.8: Tomography setup. a) first file b) second file etc

quency. This method of data acquisition was applied in previous work (i.e. Comas and Slater, 2007) and can be used for 3D reflection-model construction.

ZOP requires two separate antennas, one being used as Tx and the other as Rx. The approach used here is similar to borehole type (i.e. when used in the field, boreholes have to be drilled or dug out). Each antenna can also move independently, however in ZOP mode, both antennas (one on each boundary of the sample) are displaced at the same time and same distance, mimicking 2 antennas being lowered down in boreholes.

Tomography is the most time consuming technique of all described here. Analogous to ZOP's it requires two separate transmitter and receiver antennas. The data collection starts by fixing the location of transmitter on one surface and moving receiver along the opposite surface of the sample. Once the dataset is completed for a total of n points, where n depends on antenna separation step (2 cm in our case) and length of the survey, the transmitter is moved to the next step along the survey-line and the process is repeated (Figures 3.7 and 3.8). As a result, a full tomographic survey consists of n datafiles each one corresponding to a single transmitter location. In contrast to Common Offset Profiling (COP in figure 3.7) and ZOP's, where only one profile per one plane of investigation is needed and the end result is 1D velocity model, tomography involves several individual datasets that are later combined into one 2D velocity distribution model.



Figure 3.9: Inner structure of GPR high-frequency shielded antenna [from MALA presentation in Charleston, SC]

3.6 Ground Penetrating Radar Setup

3.6.1 Antennas

There are two types of the GPR antennas - shielded and unshielded. The only difference between them is that the shielded antennas are covered from all but one side while unshielded antennas do not have any cover and can transmit and receive electromagnetic (EM) waves in and from all the directions. The antennas used in the experiment are shielded and have a center frequency of 1.2 GHz.

Generally, GPR shielded antennas consist of bow-tie receiver (Rx) and transmitter (Tx) [Uduwawala, 2005; GPR manual] (Figure 3.9). The antennas are enclosed in rectangular cavities that serve as an absorber to reduce direct coupling [Uduwawala, 2005; Rial, 2009]. Due to the fact that some parts of antenna construction are still done by hand, even same products from one company can have slight differences in emitted wavelets or radiation patterns [Rial, 2009].

Figure 3.9 shows the interior of high frequency antennas that are similar to those used here. The size of the outer cavity of the transmitter and receiver in our experiment is approximately 11cm x 18cm x 6cm, and it is sealed and waterproof.

While each antenna has both transmitter and receiver installed inside the cavity, the ProEx Control Unit (Chapter 3.7) allows using two antennas independently, one as a trans-

mitter and the other as a receiver, when connected in a separate module. In this case, the "external Tx" option is activated and one can choose which antenna will transmit and which one will receive the signal depending on what slot (A or B) it is connected to. In this experiment slot A was used as a transmitter and slot B as receiver. Even though both antennas are identical (apart from different cover colors - black and white), the color code was used to ensure that the same antenna was always connected to the same slot. Figure 3.10 shows a representative example of the profiles acquired, showing the reflection record as antennas move along the sample holder and the EM waves propagate through air and peat.

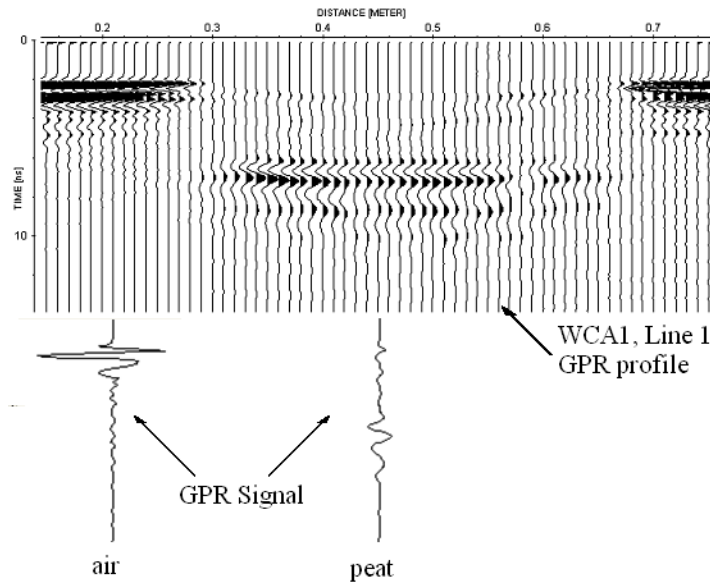


Figure 3.10: WCA1, GPR signal

Antenna Properties

Two critical properties for determining appropriateness of certain GPR antenna for a particular application are resolution and attenuation.

Resolution can be divided into two components - vertical (Δ_V) and horizontal (Δ_H). Vertical resolution allows differentiating in time two separate signals and can be easily approximated using equation 3.1, as defined by Rial (2005), where v is velocity in the

medium [Rial, 2005]:

$$\Delta_V \approx \frac{v\tau_P}{4} \quad (3.1)$$

Often $\tau_P \approx 1/f$ and equation 3.1 is substituted by equation 3.2 [Rial, 2005], where f is frequency of the signal.

$$\Delta_V \approx \frac{v}{4f} \quad (3.2)$$

Horizontal resolution indicates minimum distance between two separate and distinguishable reflectors at the same depth (equation 3.3, where z is vertical distance to the reflector)[Rial,2005].

$$\Delta_H = \sqrt{\frac{\lambda^2}{4} + \lambda z} \quad (3.3)$$

For 1.2 GHz antennas and assuming the velocity of 0.04 m/ns for the medium and maximum vertical distance of approximately 20cm, Δ_V and Δ_H can be approximated using equations 3.2 and 3.3:

$$\Delta_V \approx \frac{0.04 \cdot 10^9 m/s}{4 \cdot 1.2 \cdot 10^9 s^{-1}} \approx 0.0083m = 0.83cm \quad (3.4)$$

$$\Delta_H = \sqrt{\left(\frac{0.04 \cdot 10^9 m/s}{2 \cdot 1.2 \cdot 10^9 s^{-1}}\right)^2 + \frac{0.04 \cdot 10^9 m/s}{1.2 \cdot 10^9 s^{-1}} \cdot 0.2m} \approx 26cm \quad (3.5)$$

Note, that both equations 3.2 and 3.3 are established for one antenna configuration (transmitter and receiver are located on one side of the sample), therefore are not 100 % accurate for the two antenna ZOP measurements (Figure 3.7) due to the fact that receiver collects reflected signal in the first case and transmitted signal in the second. Hence, vertical and horizontal resolutions are expected to be smaller than the ones calculated for COP measurements. Consequently, horizontal and vertical line separations were chosen to be

approximately 4-5.5 cm.

Another thing that one has to consider when choosing antennas is antenna attenuation coefficient α (Eq. 2.4)[Neal, 2004]. As an example, for the freshwater peat relative dielectric permittivity ϵ_r is in the range of 57 and 80 and the maximum conductivity being $40 \cdot 10^{-3} \mu\text{S per m}^{-1}$, the attenuation of the 80-120 MHz GPR signal is approximately 0.3 dB per meter [Neal and Roberts, 2000]. In other words, using definition of Decibel (dB) $P_1 = 10^{\frac{-0.3\text{dB}}{10}} \cdot P_0 \approx 0.93$, where P_0 and P_1 are the strength of the signal at the surface and at 1 m depth respectively [IEEE, 2000], we can conclude that the strength of the electromagnetic signal decreases by approximately 7 % per meter for fresh water peat at a given frequency.

3.7 ProEx Control Unit

The ProEx Control unit is the fourth generation of control units from MALA and is designed to support all of the MALA antennas available both shielded and unshielded, bore-hole and high-frequency (HF). The ProEx is the administrator for the radar data collection. It consists of a power supply, a signal generating section and an internal computer [MALA Manual]. Three parallel 32-bit processors control transmitter and receiver timing, sampling and trace intervals, store all raw radar data in a temporary buffer and later transfer the data to the internal computer [MALA Manual].

The main unit is also designed for outdoor use and requires only short warm up time. It is made in aluminum and is completely waterproof [MALA Manual]. The ProEx has two module slots, A and B, where currently, three different types of antenna modules can be connected (optical, coaxial and HF). All measurements shown here were conducted with two high frequency (HF) modules. The supported antennas for this module are 1.2 GHz (used in the experiment), 1.6 GHz and 2.3 GHz.

The control unit is powered by a 12V Li-Ion battery with the capacity of 7.5V/8.8 Ah. This gives an operating time of 4 to 6 hours (approximately duration of one lab experiment).

3.8 Laboratory Measurements

The experiment was initiated on January 15th, 2010 and lasted through May 20th, 2010 (Table 3.2) with 2 to 7 days data collection intervals. Firstly, a water calibration test was performed, in order to evaluate the effects of the sample holder on EM wave travel time. An empty sample holder was filled up entirely with tap water and both a vertical and horizontal profile collected through the center of the holder (i.e. Lines 2 and B). This allowed determining the permittivity of freshwater and therefore investigating the potential errors due to both laboratory setup (i.e. sample holder geometry) and/or instrumental error.

Sample	σ , pH, TDS, T	Surface deformation	Gasmeter	Atm. pressure
WCA1	01/15 - 05/20	01/15 - 05/20	04/21 - 05/20	01/15 - 05/20
WCA2	01/15 - 05/20	01/15 - 05/20	04/21 - 05/20	01/15 - 05/20
<i>Sph</i> , GLAP	01/15 - 05/20	01/15 - 05/20	04/21 - 05/20	01/15 - 05/20
<i>Sph</i> , Maine	03/10 - 05/18	03/10 - 05/18	04/21 - 05/18	03/10 - 05/18

Table 3.2: Dates of the experiment, 2010

A total of three horizontal and three vertical ZOP profiles were collected for each of four samples (Fig.3.11). The length of the lines varies slightly for each sample because of sample holder geometry and the averages are shown in the Figure 3.11.

Lines 1, 2, and 3 correspond to the three horizontal ZOP profiles. Each profile consisted on 34 traces spaced one centimeter. Additional traces were also collected at the beginning and end of the profile through the air to correct for triggering delays as previously explained in section 3.4.

Lines A, B, and C correspond to the three vertical ZOP profiles. Following horizontal ZOPs, each profile also consisted on 34 traces spaced one centimeter. Some additional traces were also collected at the beginning and end of the profile through the air to correct for triggering delays (Section 3.4).

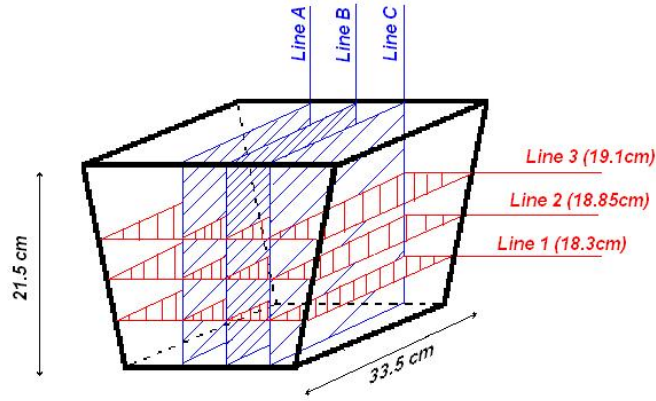


Figure 3.11: Container and line dimensions

The position of the peat block is fixed in both setups to ensure repetition within the setup for each separate survey. The change in the plane of measurements is accomplished by placing antenna elevators for horizontal setup and antenna spacers for the vertical one.

In addition, at least one horizontal and one vertical GPR tomography with 2 cm separation step (Section 3.5) was performed on each sample through the whole duration of the experiment. GPR tomography allows construction of a 2D model that contrasts with the 1D distributions of the ZOP profiles and leads to better defining spatial variability along the plane measured.

Free phase gas (FPG) concentrations were measured by GEM2000 gas meter April 27th and May 20th (Chapter 2.3.1). The measuring procedure was as follows: a known gas volume was extracted from each sample with a syringe, and slowly injected into the gas analyzer. The GEM2000 gradually pumped the gas out of the syringe, recording the maximum build up value, rather than the exact percentage of gas within the extracted volume.

Concurrently with GPR profiling surface deformation (Chapter 2.3.2), water chemistry (Chapter 2.3.3), atmospheric pressure (Chapter 2.3.4) were measured during the whole duration of the experiment. Table 3.2 shows times and durations of all measurements.

Finally porosity test was performed on June 4th (Chapter 2.3.5). Two to three small known volumes ($V_{TOTAL} = 234.76\text{cm}^3 \approx 0.23\text{L}$) of peat were extracted from each sample

and steps described in chapter 2.3.5 were executed. The porosity for each volume was calculated and averaged for each peat sample in attempt to decrease errors associated with peat volume extraction and saturation with water.

Additionally, a geochemical water analysis was performed for all samples on March 29th in order to investigate water chemistry. A total of four water samples (one for each sample) were collected and sent to an external lab (Xenco Laboratories, Boca Raton, FL) for analysis. 300 mL water samples were collected on March 29th and analyzed within 24 hours. Samples were watered with tap water (WCA) and deionized water (*Sphagnum*) on the 26th of March to ensure its saturation with any natural chemicals produced by peat. Water analysis included determination of of nitrate, nitrite, chloride, sulfate, TKN, ammonia, total phosphorus, osthophosphate, arsenic, calcium, magnesium, and dissolved methane.

3.9 Data Processing

GPR data acquisition was performed using Groundvision2 (by Mala). Groundvision2 is windows-based data collection software designed by MALA GPR systems. Among other tools it allows setting acquisition mode to one or two antenna configuration and to trigger the trace recording. All GPR data was processed using ReflexW (by Sandmeier). ReflexW (version 4.5.5) is also Windows based platform and serves as software for seismic, acoustic or electromagnetic reflection, refraction and transmission data processing. Two different modules (1D velocity analysis and modeling) were used in this research.

3.9.1 Filtering

The basic purpose of geophysical data processing is an attempt to overcome survey and data limitations in order to obtain more realistic subsurface information, which then leads to more confident interpretations and analysis of the data [Neal, 2004]. Evidently some limitations, like attenuation depth or step size, cannot be overcome by processing or should

be accounted for during the data collection, e.g. trace stacking for the ambient noise removal [Neal, 2004]. This chapter will explain the filters applied to collected data during the processing, as well as introduce necessary parameters.

Filtering sequence as applied to GPR profiles affects the final result, and although such sequence may depend on the particular nature of the measurements [Neal, 2004], it is generally accepted that processing steps that induce changes in the signal's amplitude should be applied last [Sandmeier, 1998]. The following filtering routine was used in our ZOP data analysis:

(a) subtract-mean dewow, which is used for eliminating the possible low-frequency part for each particular trace. When this option is activated and filter parameter "timerange" is set, a running mean is calculated for each trace and subtracted from the central point. Timerange is to be set by the user and can be chosen to be any positive number, however, it usually equals to the inverse of the frequency (0.8333 ns for 1.2 GHz) [Sandmeier, 1998].

(b) gain function, to enhance the signal's strength (used only in vertical profiles). This filter is used in order to compensate for possible damping or geometrical spreading losses and acts on each trace independently by multiplying it with a given function $g(t)$ (Eq. 3.6) [Sandmeier, 1998].

$$g(t) = (1 + a \cdot t) \cdot e^{b \cdot t} \quad (3.6)$$

where $a = a'/\text{pulse}$ and $b = b' \cdot v/8.69$, $v = 0.1m/ns$ and parameters a' and b' are set by the user. In this experiment, the gain parameters were set $a' = 0.5$ and $b' = 1.0$ and the pulse width is automatically taken from the nominal frequency which in turn is determined from the first arrival. Two additional parameters *starttime* and *max gain* were also set automatically although they can be changed by the user.

(c) static correction, to eliminate the signal triggering time and place the first "air" arrival at 0 ns for the tomography data. Also, in order to preserve the original amplitudes

of the traces no gain functions are used in these profiles.

3.9.2 Pickings

After all files were processed (see section 3.9.1), the time of the signal arrivals had to be picked and saved. One example of horizontal profile showing signal pickings is shown in Figure 3.12. Note that the picking was done manually for each trace and had to be consistent for all files (i.e. saved time was always the time from 0 ns to the positive lobe of the reflector for each trace).

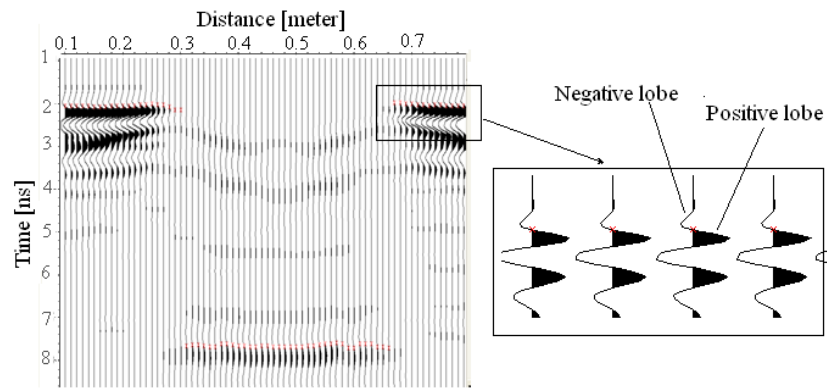


Figure 3.12: WCA1 Line 1, picking of the "air" and "peat" signals

4 Results

4.1 Ground Penetrating Radar measurements

High frequency antennas (e.g. 1.2 GHz) were used to investigate changes in travel time associated with biogenic gas build-up and release in all peat block samples. As the system is constrained in the laboratory by keeping a constant water table, any changes in travel time for the GPR signal are directly related to periods of gas build up (decrease in travel time), or release (decrease in travel time). This approach has been already proved very effective in previous research to investigate biogenic gas dynamics in the laboratory using one single high frequency antenna over a Sphagnum peat samples [Comas and Slater, 2007]. Gas content within the samples is calculated using the equation 4.1.

$$n = \frac{\phi \epsilon_w^\alpha + (1 - \phi) \epsilon_s^\alpha - \left(\frac{v}{c}\right)^{2\alpha}}{\epsilon_w^\alpha - \epsilon_a^\alpha} \quad (4.1)$$

Porosity, ϕ , is calculated using equation 2.16, relative dielectric permittivity of soil, ϵ_s , is assumed constant (2 for Florida samples and 4 for less decomposed northern peatlands samples [Kellner and Lundin, 2001 and Alayew et al., 2007]), relative dielectric permittivity of water is known (Equation 2.2) and velocity v is taken from the GPR measurements by considering distance travelled over time of the EM wave.

All GPR results appear very consistent when comparing individual samples and general trends between samples. Figures 4.1 and 4.2 show respectively results for horizontal (lines 1, 2, 3) and vertical (lines A, B, C) surveying lines together with their averages for the WCA1 Everglades sample. Gas change patterns for individual lines along each direction

mimic each other, therefore calculated three-line averages will be used for further analysis and comparison. Table 4.1 shows the average gas content for each line, which is ranging between 4% and 6% and maximum changes between 1.83% and 3.18 %. Maximum emission rates were calculated for each sample by determining gas change between neighboring minimum and maximum, and dividing by the number of days between these two measurements. Maximum emissions rates for all lines are comparable, with approximate values between 0.01 - 0.41% gas content lost per day.

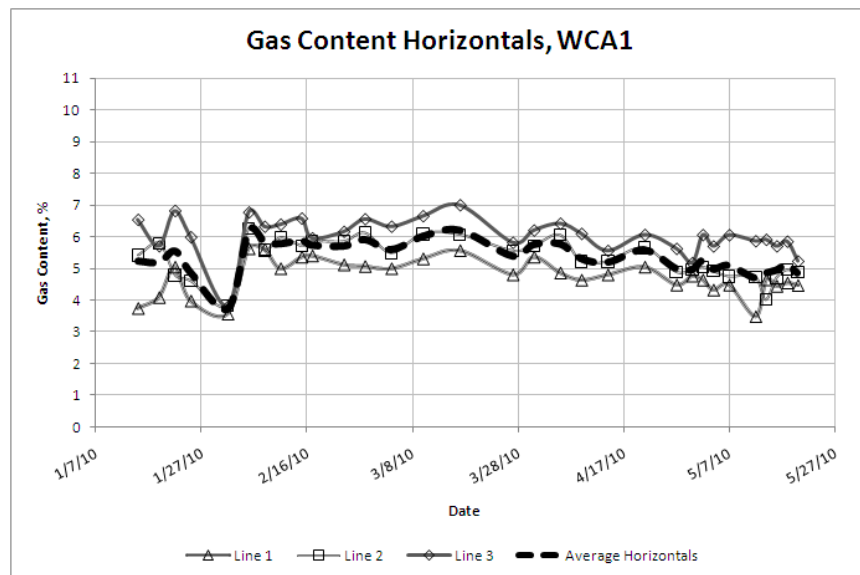


Figure 4.1: WCA1, gas content (GPR) for horizontal lines 1, 2 and 3, and their average gas content

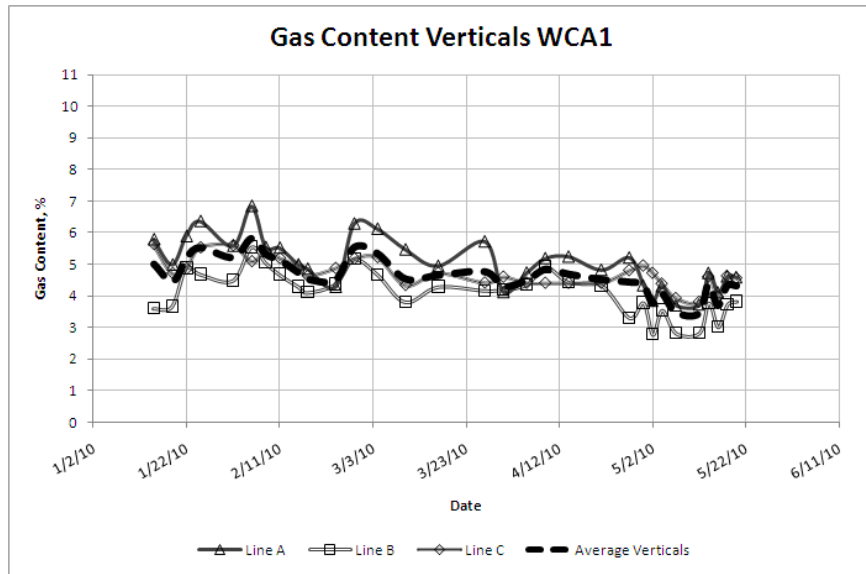


Figure 4.2: WCA1, gas content (GPR) for vertical lines A, B and C, and their average gas content

LINE	Av. Gas Content, %	Max. Gas Content, %	Max. Change, %	Max. emission rate % per day
Line 1	4.75	5.62	2.12	0.30
Line 2	5.31	6.26	2.44	0.11
Line 3	6.02	6.99	3.18	0.40
Line A	5.03	6.84	3.16	0.40
Line B	4.11	5.55	2.77	0.11
Line C	4.73	5.63	1.83	0.12

Table 4.1: WCA1 average, maximum gas content, maximum change and emission rate

Figures 4.3 and 4.4 show results for horizontal (lines 1, 2, 3) and vertical (lines A, B, C) surveying lines respectively together with their averages for the WCA2 Everglades sample. Again, gas change patterns for individual lines along each direction mimic one another and

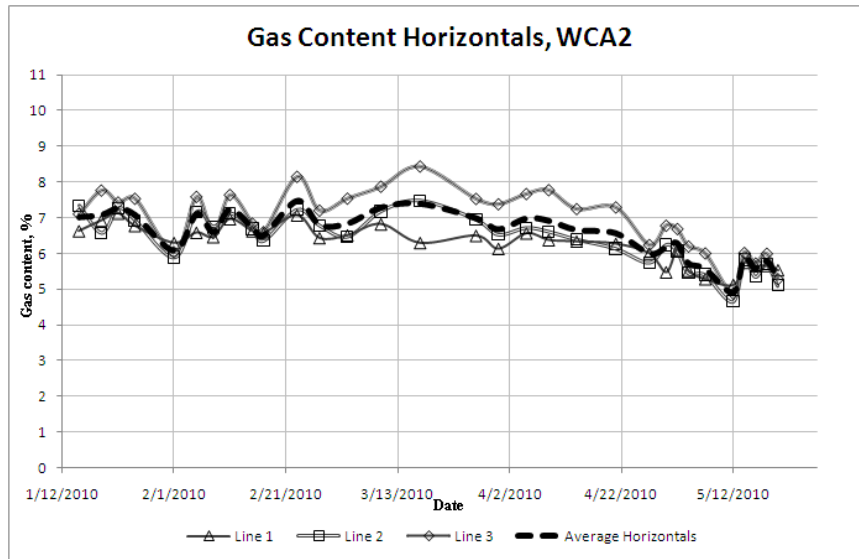


Figure 4.3: WCA2, gas content (GPR) for horizontal lines 1, 2 and 3, and their average gas content

the calculated three-line averages will be used for further analysis and comparison. Table 4.2 shows the average gas content for each line and shows the consistency within all results with average gas content values ranging between 4.82% and 6.94 % and maximum changes between 1.38% and 3.55%. Maximum emission rates for all lines are comparable to those for the previous sample (WCA1) and show approximate values between 0.08 - 0.22% gas content loss per day.

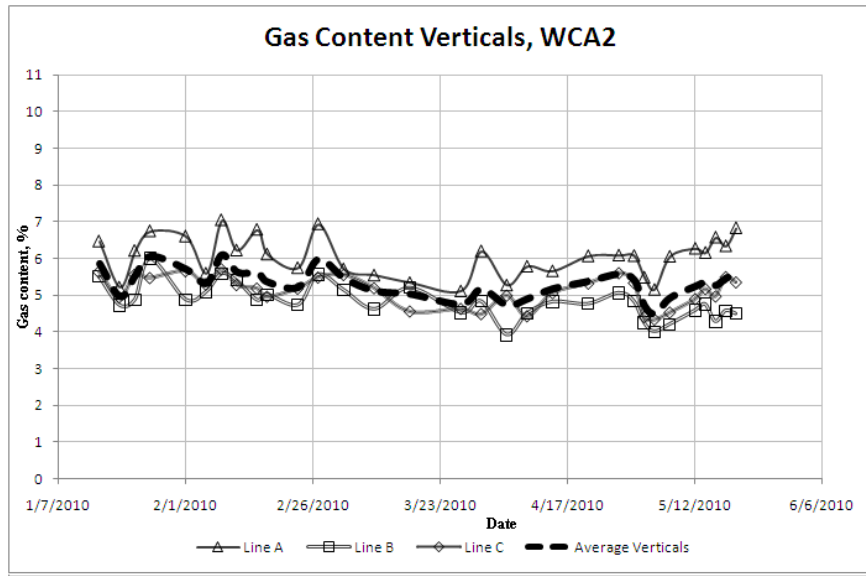


Figure 4.4: WCA2, gas content (GPR) for vertical lines A, B and C, and their average gas content

LINE	Average Content, %	Max. Gas Content, %	Max. Change, %	Max. emission rate % per day
Line 1	6.26	7.12	2.00	0.09
Line 2	6.39	7.48	2.82	0.19
Line 3	6.94	8.44	3.55	0.22
Line A	6.05	7.04	1.91	0.10
Line B	4.82	5.99	2.07	0.16
Line C	5.12	5.72	1.38	0.08

Table 4.2: WCA2 average, maximum gas content, maximum change and emission rate

Figures 4.5 and 4.6 show respectively results for horizontal (lines 1, 2, 3) and vertical (lines A, B, C) lines together with their averages for the *Sphagnum* Minnesota sample. Following the analysis for all previous samples, a three-line average was calculated for each direction and will be used for further analysis and comparison. Table 4.3 shows the

average gas content for each line and shows the consistency within all results with average gas content values ranging between 4.5% and 6.12 % and maximum changes between 4.99% and 7.69%. The sample shows a gradual gas buildup over the entire experiment. Maximum emission rates for all lines are again comparable between lines as well as all previous samples, with approximate values between 0.09 - 0.41% gas content loss per day.

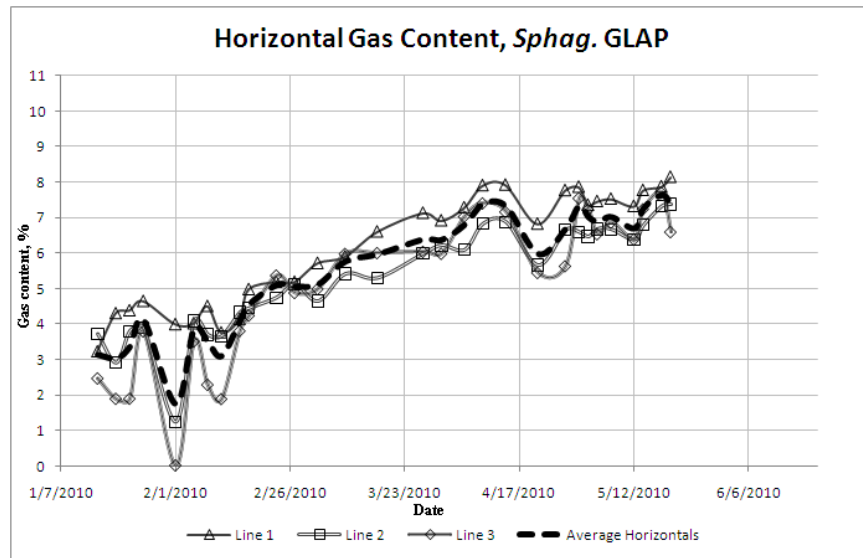


Figure 4.5: *Sphagnum* (GLAP), gas content (GPR) for horizontal lines 1, 2 and 3, and their average gas content

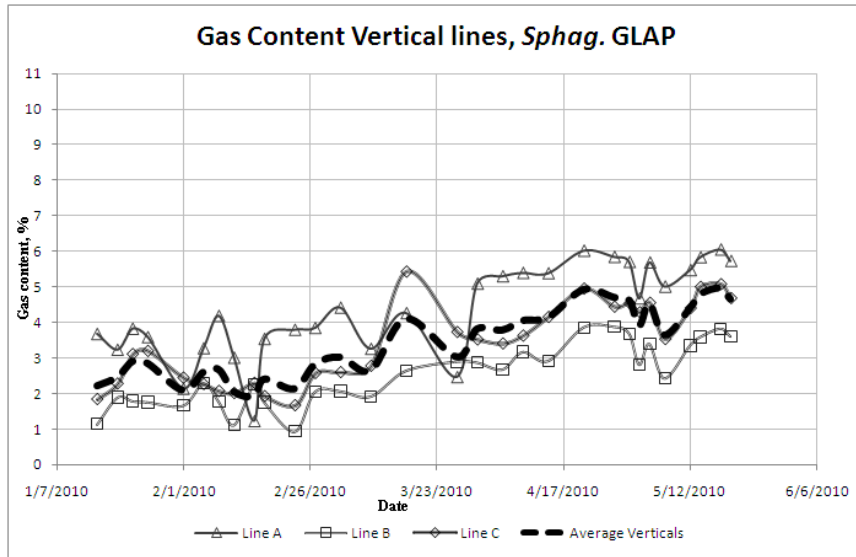


Figure 4.6: *Sphagnum* (GLAP), gas content (GPR) for vertical lines A, B and C, and their average gas content

LINE	Average Gas Content, %	Max. Gas Content, %	Max. Change, %	Max. emission rate % per day
Line 1	6.12	8.14	4.90	0.09
Line 2	5.32	7.37	6.13	0.38
Line 3	5.13	7.71	7.69	0.39
Line A	5.47	7.12	4.72	0.41
Line B	3.67	4.99	2.90	0.09
Line C	4.54	6.54	3.73	0.11

Table 4.3: *Sphagnum*, GLAP, average, maximum gas content, maximum change and emission rate

Figures 4.7 and 4.8 show respectively results for horizontal (lines 1, 2, 3) and vertical (lines A, B, C) surveying lines together with their averages for the *Sphagnum* Maine sample. Although the survey was much shorter for this sample as compared to the previous

ones, gas patterns for individual lines are again very consistent as shown by the calculated three-line averages. Table 4.4 shows the average gas content for each line and shows the consistency within all results with average gas content values ranging between 4.6% and 7.96 % and maximum changes between 7.49% and 10.26%. Similar to the previous *Sphagnum* sample, gas content shows gradual buildup over the duration of the experiment. Maximum emission rates for all lines are comparable with approximate values between 0.01 - 0.27% gas content loss per day.

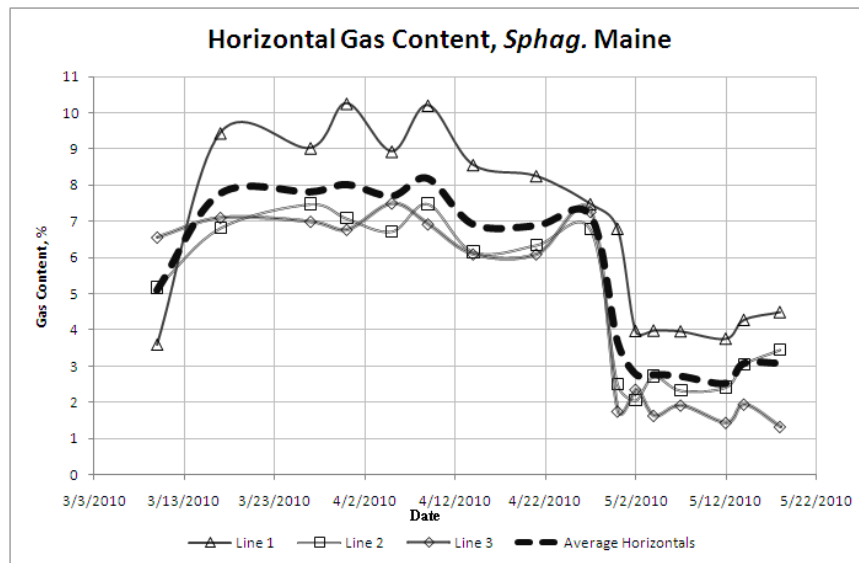


Figure 4.7: *Sphagnum* (Maine), gas content (GPR) for horizontal lines 1, 2 and 3, and their average gas content

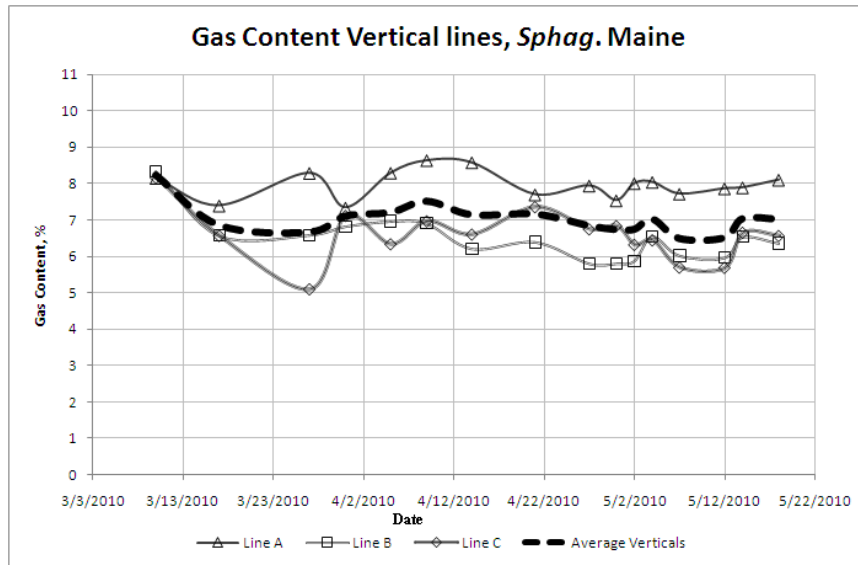


Figure 4.8: *Sphagnum* (Maine), gas content (GPR) for vertical lines A, B and C, and their average gas content

LINE	Average Gas Content, %	Max. Gas Content, %	Max. Change, %	Max. emission rate % per day
Line 1	6.69	10.26	6.66	0.16
Line 2	4.91	7.49	5.44	0.27
Line 3	4.60	7.50	6.19	0.07
Line A	7.96	8.68	1.29	0.01
Line B	6.48	8.34	2.54	0.01
Line C	6.57	8.17	3.08	0.01

Table 4.4: *Sphagnum*, Maine, average, maximum gas content, maximum change and emission rate

Figures 4.13 and 4.14 show average gas content variability for each sample. Both vertical and horizontal line averages of GPR measurements follow similar trends and major

increases of atmospheric pressure (like on February 1st and March 4th) are consistently associated with drops in gas content for each sample (See section 5.1).

Overall, *Sphagnum* samples show higher maximum gas contents but maximum emission rates are comparable among all the samples. For WCA2 and both *Sphagnum* samples, horizontal lines show higher emission rates, and only WCA1 sample demonstrate comparable gas release rates for all lines. *Sphagnum* (Maine) sample shows the largest gas content (10.26 %) and the maximum emission (6.7%), which is further discussed in next chapter.

4.2 Ebullition events and surface deformation measurements

Surface deformation measurements show overall consistent results and a particularly good correspondence with GPR gas content variability along vertical lines (Figures 4.9, 4.10, 4.11 and 4.12). These plots are also compared to atmospheric pressure results as measured in the laboratory.

WCA1 shows four major drops in gas content for the average horizontal lines on February 1st, February 11th, March 27th and May 12th, and four decreases for average vertical lines on February 1st, February 23rd, March 30th and May 12th, that are coincident with the atmospheric pressure increases as indicated in figure 4.9 (note, that throughout the thesis, the atmospheric pressure axis is inverted for better visual correspondence with gas content). Hence, on February 1st 7 mbar pressure increase is associated with gas content decreases of 1.6% for horizontal lines and 0.4% for vertical lines and a surface deformation decrease of 0.3cm. On February 11th - 23rd, 6 mbar increase caused 0.4% and 1.0% decrease in horizontal and vertical lines respectively plus a surface deformation decrease of 0.02cm - 0.12cm. On May 12th 9.6 mbar increase coincides with 0.9% gas drop for horizontal lines and before that 5 mbar atmospheric pressure increase matched with 0.9% gas emission for vertical lines with a surface deformation decrease of 0.01cm (Fig. 4.9).

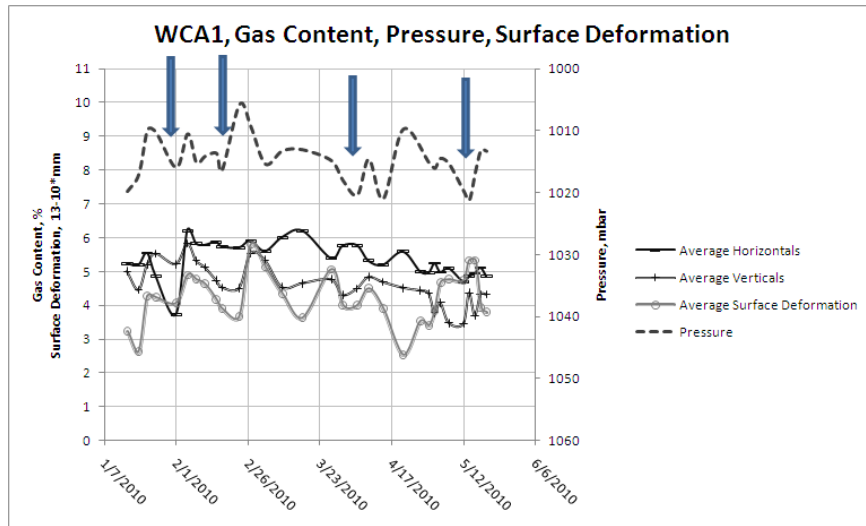


Figure 4.9: WCA1, Average Gas Content (GPR) for horizontal and vertical lines, Surface Deformation and Pressure (pressure axis is inverted), arrows indicating increase in atm. pressure match with gas content drops

WCA2 shows four major drops (February 1st, February 17th, February 27th, May 12th) in average horizontal lines gas contents and four drops for verticals (February 5th, February 23rd, March 27th, April 2nd, May 4th). For horizontals, 7 mbar, 3 mbar, 10 mbar and 4 mbar increases of atmospheric pressure are associated with 1.3% 0.7% and 1.7% and 0.6 % of gas release respectively and surface deformation decrease of 0.09 cm, 0.01 cm, -0.02 cm and -0.12 cm; 7 mbar, 4 mbar, 6 mbar and 5 mbar pressure increase for verticals coincide with gas content drops of 0.8 %, 0.9 %, 1.2%, and 1.1%, and surface deformation decreases of 0.1cm, 0.03cm, 0.01cm and 0.01cm respectively(Fig.4.10).

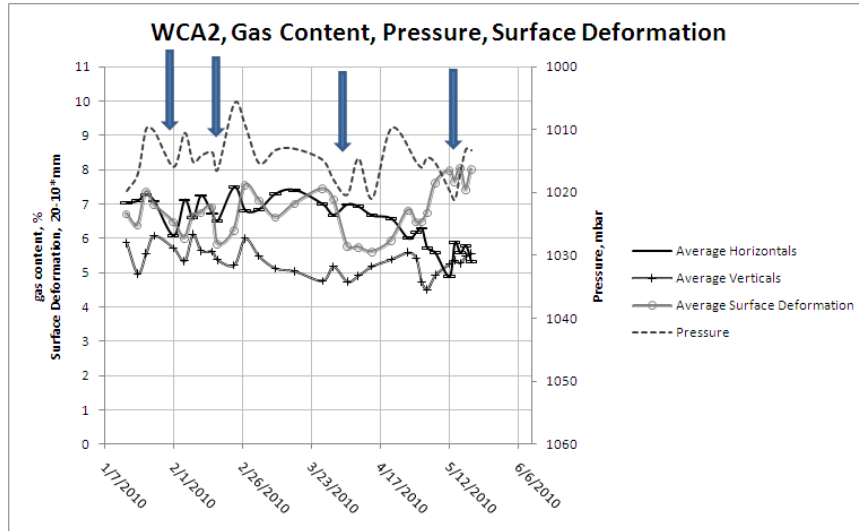


Figure 4.10: WCA2, Average Gas Content (GPR) for horizontal and vertical lines, Surface Deformation and Pressure (pressure axis is inverted), arrows indicating increase in atm. pressure match with gas content drops

Sphagnum, (GLAP) samples show remarkable consistency between horizontal and vertical lines, atmospheric pressure and surface deformation. Major gas content drops for both lines (February 1st, February 11th-15th, May 7th-12th) of 1.7%, 0.7%, 0.64% for horizontal lines and 0.8%, 0.7%, and 1.2% for vertical lines corresponded with 7 mbar, 5 mbar, 5-10 mbar atmospheric pressure increases. Surface deformation also shows corresponding decreases of 0.03 - 0.11cm, 0.03cm and 0.01 cm (Fig. 4.11).

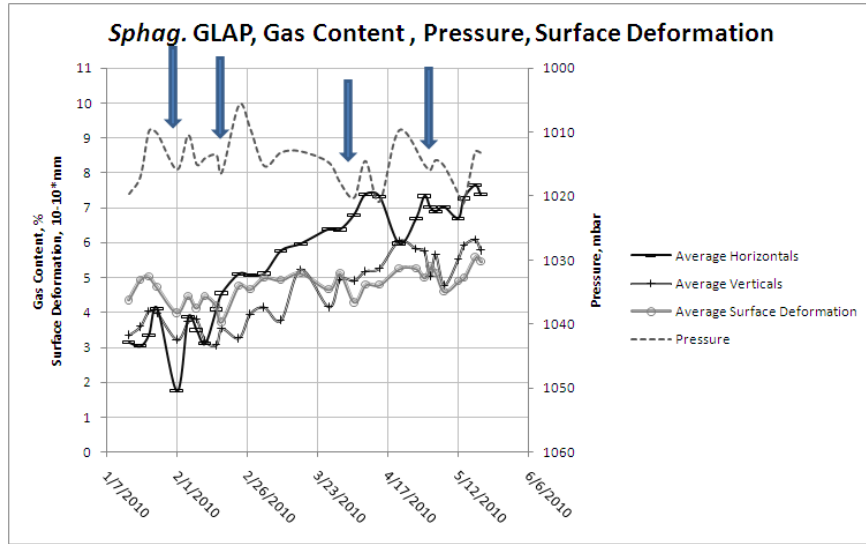


Figure 4.11: *Sphagnum* (GLAP), Average Gas Content (GPR) for horizontal and vertical lines, Surface Deformation and Pressure (pressure axis is inverted), arrows indicating increase in atm. pressure match with gas content drops

Sphagnum (ME) was included in the experiment in March and was investigated for only 58 days (in contrast to 125 days measurements for other samples). Nevertheless, we can distinguish three major gas release events that match with atmospheric pressure and surface deformation curves. Three drops of gas content in horizontal lines (April 5th, April 14th, May 12th) and three in vertical lines (April 14th, April 30th, May 7th) of 0.3%, 1.3%, 5.0% and 0.4%, 0.4% and 0.5% respectively are associated with 2 mbar, 7 mbar and 11 mbar atmospheric pressure increases and surface deformation decreases of 0.1 cm, 0.11 cm and 0.32cm (Figure 4.12).

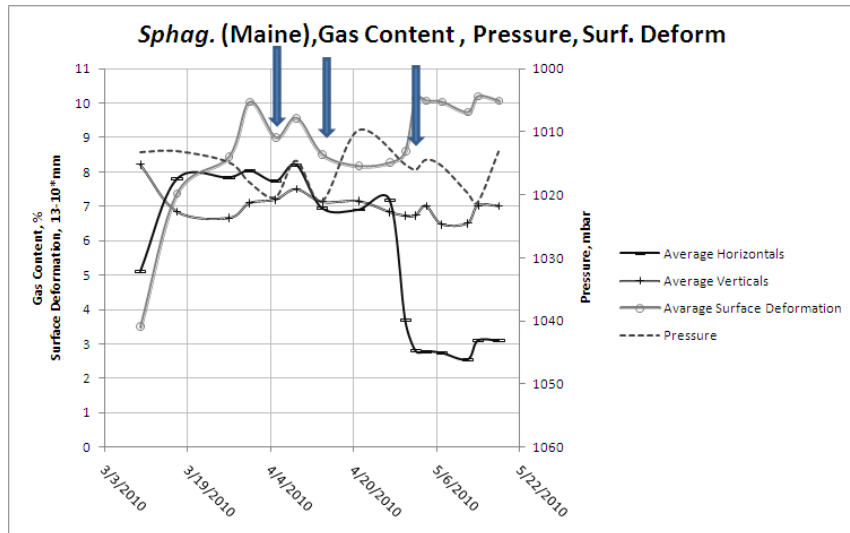


Figure 4.12: *Sphagnum* (Maine), Average Gas Content (GPR) for horizontal and vertical lines, Surface Deformation and Pressure (pressure axis is inverted), arrows indicating increase in atm. pressure match with gas content drops

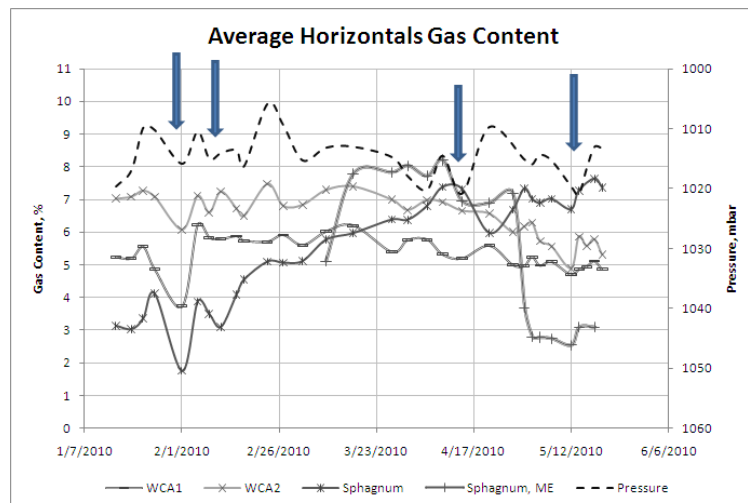


Figure 4.13: Horizontal lines' Average GPR gas content: WCA1, WCA2, *Sphagnum* (GLAP), *Sphagnum* (Maine) and atmospheric pressure (axis inverted), arrows indicating increase in atm. pressure match with gas content drops

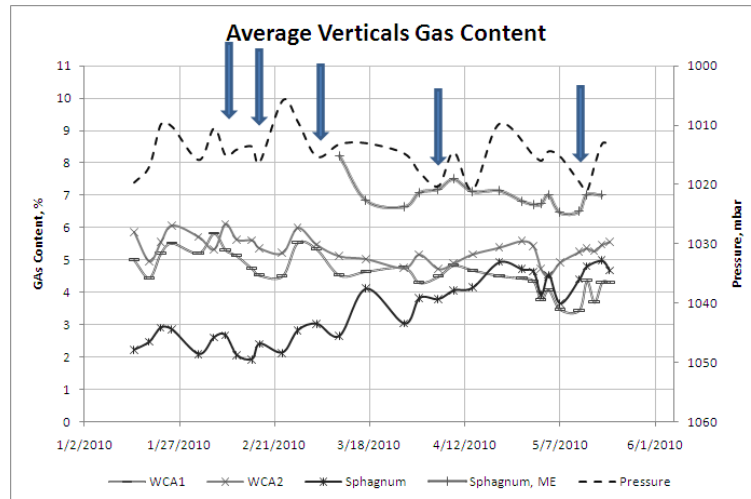


Figure 4.14: Vertical lines' Average GPR gas content: WCA1, WCA2, *Sphagnum* (GLAP), *Sphagnum* (Maine) and atmospheric pressure (axis inverted), arrows indicating increase in atm. pressure match with gas content drops

Tables 4.5, 4.6, 4.7 and 4.8 show horizontal and vertical lines' (H or V) GPR gas content increases for WCA1, WCA2, *Sphagnum*, GLAP and *Sphagnum* Maine samples respectively along with time period, atmospheric pressure increase and surface deformation decrease (negative numbers correspond to pressure decrease or deformation increase). All four tables are divided into two tables; the top table corresponds to gas emission volumes calculated from more than 2 datapoints and the bottom table corresponds to gas volumes established from 2 consecutive measurements.

Line	Dates	GPR, gas drop	Atm. pressure increase	Surface deformation
Three and more consecutive datapoints				
H	01/22-02/01	1.6 %	7 mbar	0.30 cm
H	02/05-02/11	0.4 %	5 mbar	0.02 cm
V	02/05-02/23	1.0 %	6 mbar	0.12 cm
H	04/21-05/12	0.9 %	10 mbar	0.22 cm
V	04/14-05/02	0.9 %	5 mbar	0.01 cm
Two consecutive datapoints				
V	01/25-02/01	0.4 %	5-6 mbar	0.30 cm
V	03/04-03/10	0.8 %	2 mbar	0.08 cm
V	03/17-03/27	0.8 %	2 mbar	-0.10 cm
H	03/27-03/31	0.4 %	3 mbar	0.11 cm

Table 4.5: WCA1 dates and percentage of gas emissions, corresponding atmospheric pressure increase and surface deformation

Line	Dates	GPR, gas drop	Atm. pressure increase	Surface deformation
Three and more consecutive datapoints				
H	01/22-02/01	1.3 %	7 mbar	0.09 cm
V	01/25-02/05	0.8 %	7 mbar	0.10 cm
H	02/11-02/17	0.7 %	2-3 mbar	0.10 cm
V	02/08-02/23	0.9 %	4 mbar	0.03 cm
V	02/27-03/27	1.2 %	6 mbar	0.01 cm
H	04/21-05/12	1.7 %	10 mbar	-0.2 cm
V	04/27-05/04	1.1 %	5 mbar	0.01 cm
Two consecutive datapoints				
H	02/23-02/27	0.6 %	4 mbar	-0.12 cm

Table 4.6: WCA2 dates and percentage of gas emissions, corresponding atmospheric pressure increase and surface deformation

Line	Dates	GPR, gas drop	Atm. pressure increase	Surface deformation
Three and more consecutive datapoints				
V	01/22-02/01	0.8 %	7 mbar	0.11 cm
H	02/05-02/11	0.7 %	5 mbar	0.00 cm
V	02/05-02/15	0.7 %	3 mbar	0.03 cm
H	04/09-05/12	1.4 %	6 mbar	0.00 cm
H	04/30-05/12	0.6 %	5 mbar	0.01 cm
V	04/21-05/07	1.2 %	10 mbar	0.07 cm
Two consecutive datapoints				
V	01/25-02/01	1.7 %	6 mbar	0.03 cm
H	03/17-03/27	1.1 %	2 mbar	0.05 cm

Table 4.7: *Sphagnum*, GLAP dates and percentage of gas emissions, corresponding atmospheric pressure increase and surface deformation

Line	Dates	GPR, gas drop	Atm. pressure increase	Surface deformation
Three and consecutive datapoints				
V	04/21-05/30	0.4 %	5 mbar	-0.03 cm
V	04/27-05/12	5.0 %	11 mbar	0.32 cm
Two consecutive datapoints				
H	03/31-04/05	1.3 %	7 mbar	0.11 cm
H	04/09-04/14	0.4 %	6 mbar	0.31 cm
V	03/31-04/05	0.3 %	2 mbar	0.10 cm
H	05/04-05/07	0.5 %	1 mbar	0.01 cm

Table 4.8: *Sphagnum*, ME dates and percentage of gas emissions, corresponding atmospheric pressure increase and surface deformation

Assuming that 54.0% of biogenic gas volume is methane [Glaser et al., 2004], and that 7% is carbon dioxide [Chanton et al., 1988] with the remaining 39% corresponding mostly to nitrogen, N_2 and oxygen, O_2 [Chanton et al., 1988] and by approximating (a) the surface area of the peat block to be 0.067 m^2 ; and (b) the total volume of gas emitted from each sample individually equals $3 \cdot V_A$, where V_A is volume of emitted gas calculated from the average GPR measurements of three vertical lines (A, B and C), we can estimate the rate ebullition per square meter of the surface per one event using ideal gas law (Eq. 4.2) to estimate the mass of the emitted gas.

$$PV = nRT \quad (4.2)$$

Estimating an average pressure to be 0.9995 atm, average temperature of 293.8 K, and $n = \frac{M}{m_{mol}}$, $m_{CH_4} = 16$ and $m_{CO_2} = 44$, the emission rates, E_{CH_4} and E_{CO_2} , for each sample can be measured (Eq. 4.3, where gas flux (or emission) Φ is defined as $\Phi = M/A$ with M being mass in mg and A being total surface area of the sample measured in m^2).

$$E = \frac{\Phi}{N_{days}} = \frac{M}{A \cdot N_{days}} \quad (4.3)$$

In this section, the emission rates of the sum of both CH_4 and CO_2 is going to be used with a combined units of mgC/m^2 per day for a single ebullition event, constrained by a single major atmospheric pressure increase. Examples of calculations are shown below (Eq. 4.4, 4.5 and 4.6).

$$E_{CH_4} = \frac{P \cdot V(CH_4) \cdot m_{mol}}{N_{days} \cdot A_{total} \cdot RT} = \frac{0.58L \cdot 3 \cdot 0.54 \cdot 0.995atm \cdot 16mol}{0.067m^2 \cdot R \cdot 298.3K} = 70.42mg \cdot m^{-2} \quad (4.4)$$

$$E_{C-CH_4} = \frac{E_{CH_4}}{16} \cdot 12 \quad (4.5)$$

$$E_{C-CO_2} = \frac{E_{CO_2}}{44} \cdot 12 \quad (4.6)$$

Table 4.9 shows four such events and rates of biogenic gas fluxes calculated from GPR data along with atmospheric pressure increases and surface deformation decreases. *Italic font* represents results received from 2-datapoint ebullition events and *normal font* corresponds to the results of 3 and more datapoints.

Figures 4.15, 4.16, 4.17 and 4.18 show all four gas emission events for each sample respectively. Each event is labeled on the plot and assigned green color for the first event, violet for the second, blue for the third and yellow for the fourth event.

Sample	Event 1 (01/22 - 02/05/2010)					Event 2 (02/05 - 02/23/2010)				
	N days	Gas lost, %	Flux rate, mgC/m^2 per day	Atmosph. Pressure, mbar	Surf. deform., cm	N days	Gas lost, %	Flux rate mgC/m^2 per day	Atmosph. Pressure, mbar	Surf. deform., cm
WCA1	6	0.4.3	130.41	5.0	0.30	18	1.0.3	108.66	6.0	0.12
WCA2	9	0.8.3	163.02	7.0	0.10	15	0.9.3	186.63	3.6	0.03
Sph., GLAP	10	0.8.3	156.51	7.0	0.11	10	0.7.3	136.92	3.0	0.03
Sph., ME	-	-	-	-	-	-	-	-	-	-
Sample	Event 3 (02/27 - 03/17/2010)					Event 4 (04/21 - 05/14/2010)				
	N days	Gas lost, %	Flux rate, mgC/m^2 per day	Atmosph. Pressure, mbar	Surf. deform., cm	N days	Gas lost, %	Flux rate mgC/m^2 per day	Atmosph. Pressure, mbar	Surf. deform., cm
WCA1	6	0.8.3	195.63	2.0	0.08	18	0.9.3	99.99	5.0	0.01
WCA2	28	1.2.3	83.85	5.5	0.01	7	1.1.3	307.41	5.0	0.01
Sph., GLAP	10	1.1.3	215.19	6.0	0.03	16	1.2.3	151.59	10.0	0.07
Sph., ME	17	1.5.3	176.45	1.6	-0.45	9	0.4.3	86.94	5.0	-0.03

Table 4.9: Gas flux rates estimated from GPR data per one ebullition event along with atmospheric pressure increase and surface deformation decrease for each peat sample (amount of gas is multiplied by three to approximate gas ebullition from all three vertical lines)

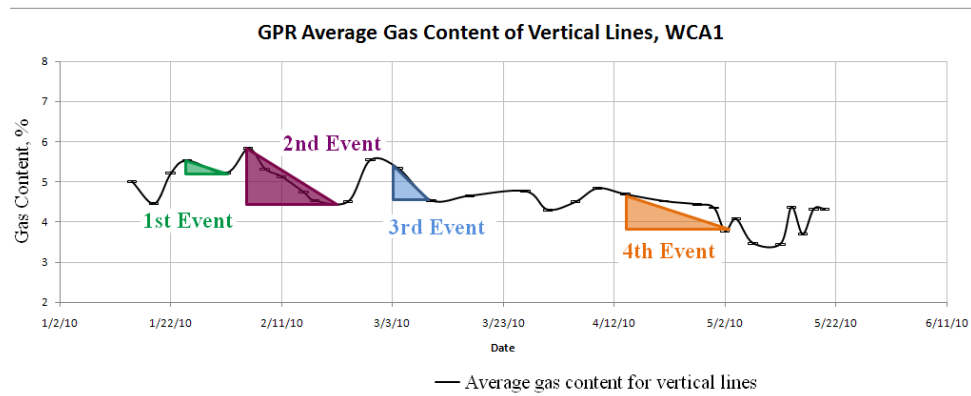


Figure 4.15: WCA1 four major gas ebullition events (1st - green, 2nd - violet, 3rd - blue, 4th - yellow)

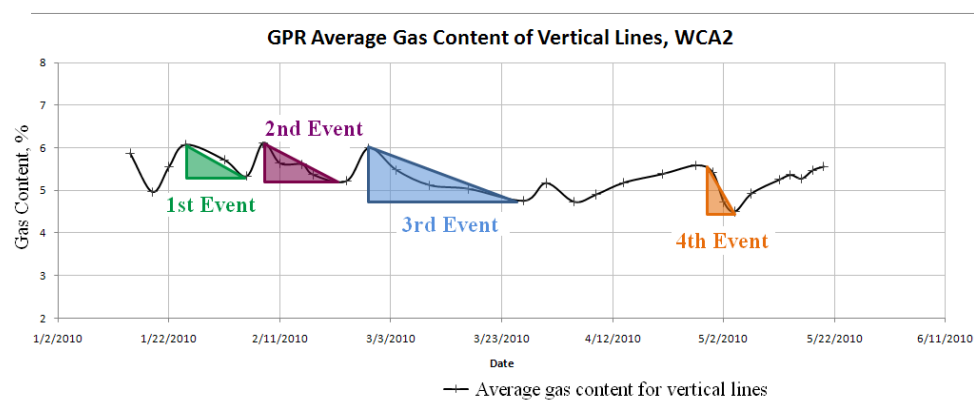


Figure 4.16: WCA2 four major gas ebullition events (1st - green, 2nd - violet, 3rd - blue, 4th - yellow)

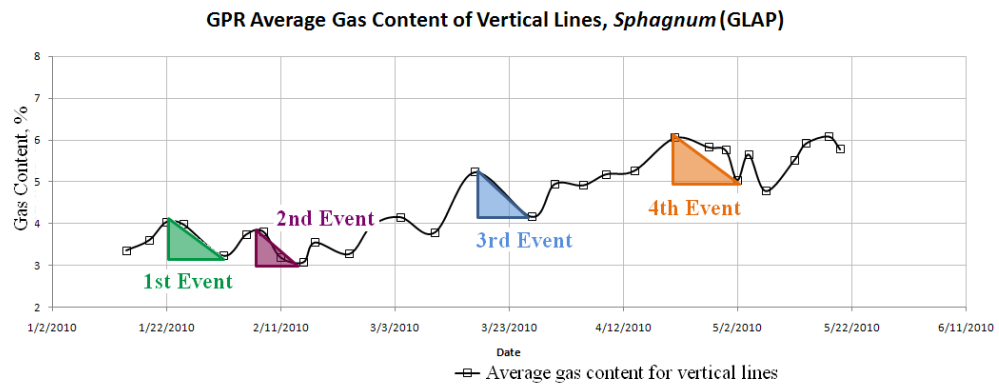


Figure 4.17: *Sphagnum*, GLAP four major gas ebullition events (1st - green, 2nd - violet, 3rd - blue, 4th - yellow)

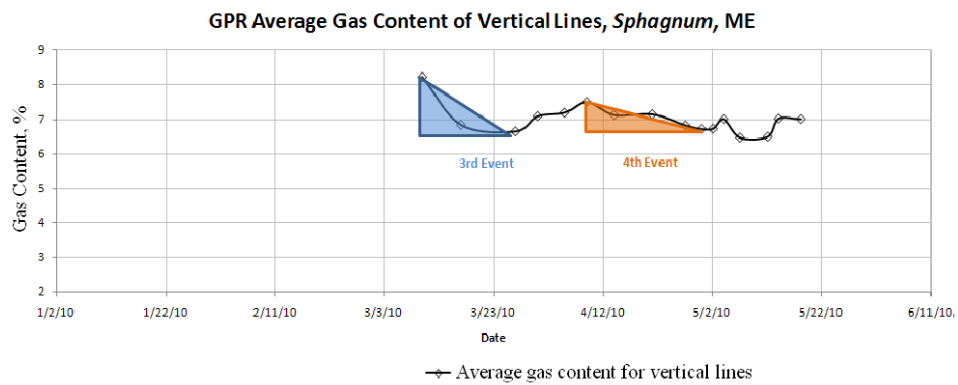


Figure 4.18: *Sphagnum*, Maine four major gas ebullition events (1st - green, 2nd - violet, 3rd - blue, 4th - yellow)

4.3 Gas meter measurements

Given the restrictions with equipment availability (the GEM 2000 was rented weekly), gas meter measurements were collected only during the last 4 weeks of the experiment and consisted of 10 datapoints. Due to low sampling frequency of the GEM2000 and the difficulty of directly measuring FPG fluxes, the calculated concentrations may not represent the real concentrations of the gasses within the sample. However, the results represent a qualitative

measure of gas content within the sample and proved (a) the existence of biogenic gas (i.e. methane and carbon dioxide in all samples); (b) showed that methane is the dominant gas between the two. Figures 4.19, 4.20, 4.21 and 4.22 show the results for extracted concentrations of methane and carbon dioxide for samples WCA1, WCA2, *Sphagnum* GLAP and *Sphagnum* Maine respectively and collected during a four week period. The results in each case are plotted together with GPR gas measurements for comparison.

Figures 4.19, 4.20, 4.21 and 4.22 show the results of Gas Meter measurements (i.e. bulk concentrations of CO_2 and CH_4) and GPR measurements for the same dates for WCA1, WCA2, *Sphagnum* from GLAP and *Sphagnum* from Maine samples respectively with the arrows indicating consistent trends between the two measurements.

WCA1 sample shows the most consistent results between GPR and gas meter measurements. The arrows in figure 4.19 indicates the correspondence between GPR and gas-meter gas content measurements for WCA1 sample. Decreases in GPR vertical gas content during May 2nd, May 7th, and May 16th correspond to decreases of average gas concentrations, and increases in GPR vertical and horizontal gas contents on May 14th and May 18th coincide with gas concentration increases.

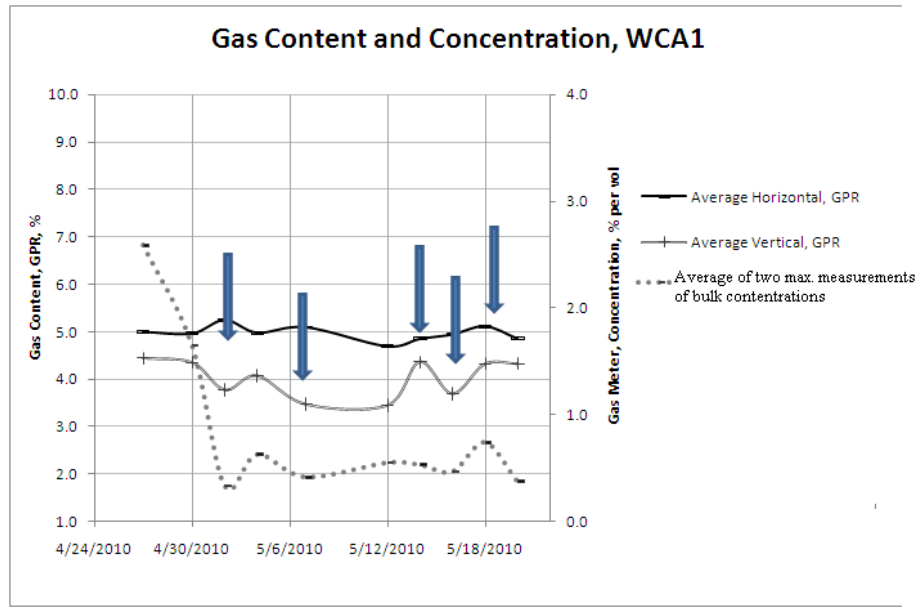


Figure 4.19: Gas Meter Measurements (average of two bulk concentrations (CH_4 and CO_2) measurements) and GPR Data, WCA1, arrows indicating dates of similar trends in GPR and gas meter measurements

The arrows in figure 4.20 indicates the correspondence between GPR gas content and gas-meter measurements in sample WCA2. Decreases in GPR vertical and horizontal gas contents during the days May 4th, May 16th correspond to decreases in average gas concentrations, and increase in GPR horizontal gas content during May 2nd coincides with gas concentration increase.

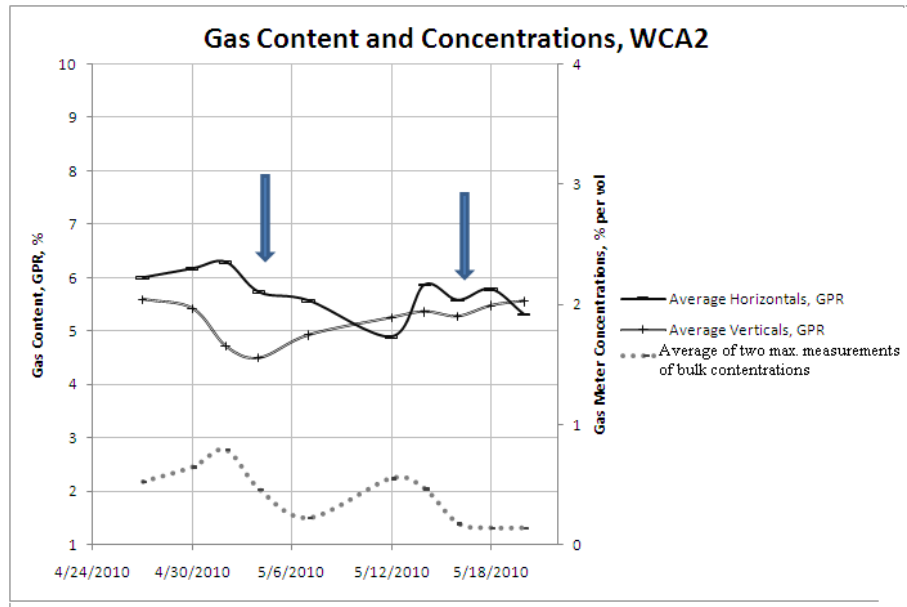


Figure 4.20: Gas Meter Measurements (average of two bulk concentrations (CH_4 and CO_2) measurements) and GPR Data, WCA2, arrows indicating dates of similar trends in GPR and gas meter measurements

The arrows in figure 4.21 indicate correspondence between GPR and gas meter measurements for *Sphagnum* (GLAP) sample. Decrease in GPR vertical gas contents on May 8th corresponds to decrease of average gas concentration, and increases in GPR vertical and horizontal gas contents on May 12th and May 18th coincide with gas concentration increases.

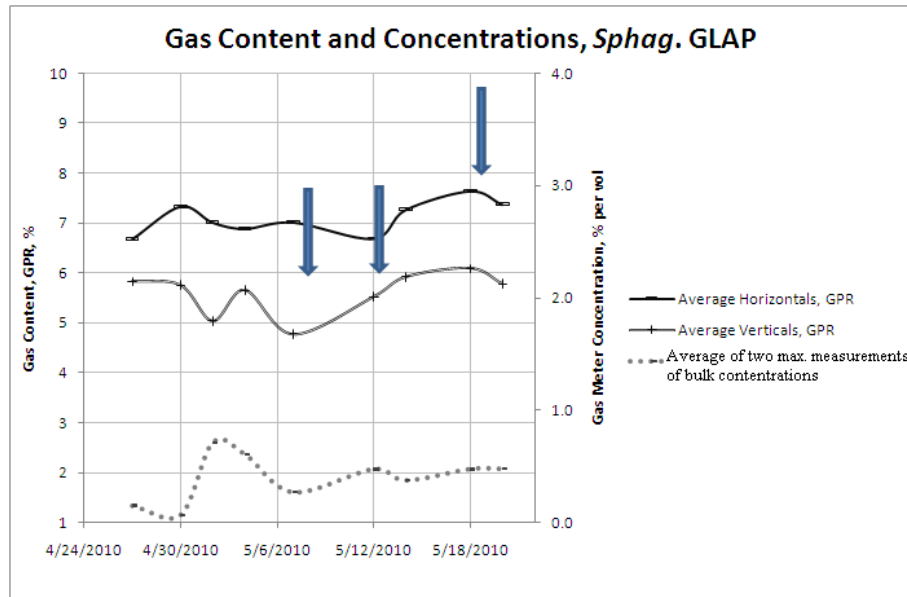


Figure 4.21: Gas Meter Measurements (average value of two measurements of bulk concentrations of CH_4 and CO_2) in comparison with GPR Data, *Sphagnum* (GLAP), arrows indicating dates of similar trends in GPR and gas meter measurements

The arrows on the figure 4.22 point out the consistency between gas meter and GPR measurements, hence the drops in GPR vertical and horizontal gas contents on March 30th and May 12th mimic the drops of average FP gas concentrations, and increase in GPR vertical and horizontal average gas content during May 15th coincide with gas concentration increase.

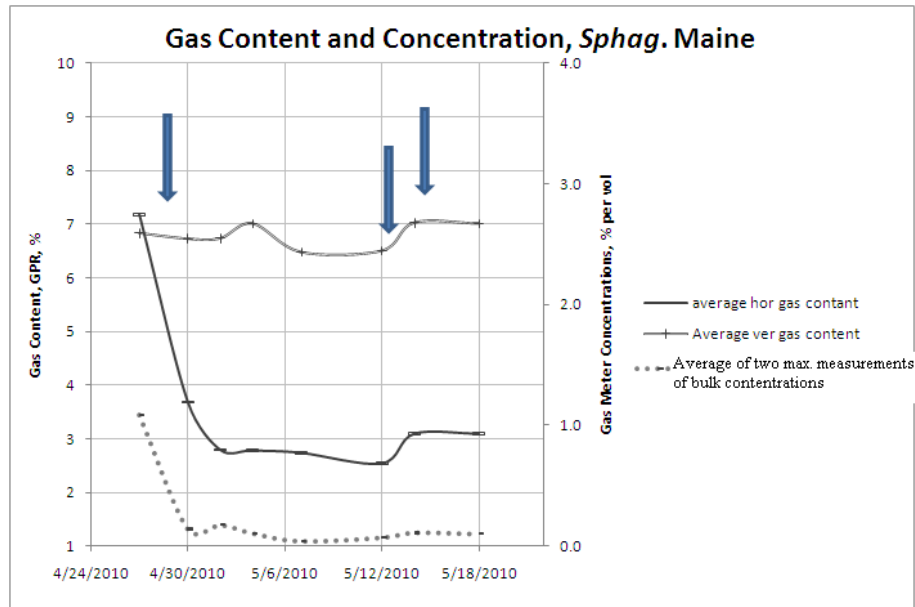


Figure 4.22: Gas Meter Measurements (average value of two bulk concentrations measurements of CH_4 and CO_2) in comparison with GPR Data, *Sphagnum* (Maine), arrows indicating dates of similar trends in GPR and gas meter measurements

Table 4.10 shows maximum CH_4 and CO_2 concentrations measured in % per volume for all 4 samples. Methane to carbon dioxide ratio is smaller for Florida samples in comparison with the *Sphagnum* samples, therefore showing methane concentrations generally much higher than carbon dioxide concentrations [i.e. Rosenberry, 2006]. Everglades samples show larger gas concentrations, which is also consistent with the dissolved gas measurements in table 4.11 (Chapter 4.4).

Sample	CH_4 concentration, % per vol	CO_2 concentration, % per vol
WCA1	3.43	0.49
WCA2	2.20	0.91
<i>Sphagnum</i> , GLAP	0.35	0.27
<i>Sphagnum</i> , ME	0.70	0.47

Table 4.10: Maximum CH_4 and CO_2 concentrations (% per vol) for all peat samples

4.4 Water chemistry analysis

The results of the water test (Chapter 3.8) are presented in the table 4.11 as concentrations of each chemical for all for samples. The units used are mg/L.

mg/L	Sample A	Sample B	Sample C	Sample D
	<i>Sphagnum</i> (ME)	<i>Sphagnum</i> (GLAP)	WCA1	WCA2
Calcium	2.26	1.31	25	52.7
Magnesium	0.749	0.524	6.7	11.7
Ortho-Phosphate	1.82	0.576	4.45	-
Total Phosphorus	2.873	0.8472	5.464	-
Dissolved Methane	-	0.322	1.44	0.698

Table 4.11: Results of water analysis

Calcium and Magnesium are rarely objects of regulatory concern, because under most circumstances they do not pose any toxicity threat. Nevertheless, they have an important role in wetland functioning. The results of our testing are in the range for average concentration of inland waters of different hardness (higher concentration of dissolved minerals implies larger hardness), which is 0.3 - 70 mg/L for calcium and 0.4 - 40 mg/L for magnesium [Kadlec et al., 2009].

Sulfate can be associated with natural inflow, fossil fuels [Novakov et al., 2002], presence of volcanoes [Lee, 1996] and mining. The minimum concentration of dissolved sulfate in our samples is 3.19 mg/L for *Sphagnum* Sample from Minnesota, and the maximum is 26.8 mg/L for Florida Peat Block from Water Conservation Area 2.

All Phosphates are naturally occurring form of element Phosphorus (P) [Kuntz, 2006]. In freshwater ecosystems, phosphorus is described as major limiting nutrient and under natural conditions is short in supply. The limit of P in soil is 300 lbs/acre [Daniels et al., 1997] which is equivalent to approximately 0.55 mg/L of dissolved reactive phosphorus [Sharpley, 1993]. The concentrations of P in 3 out of 4 of our samples are higher than this limit, but we have to note again that the criterion has been debated for several years now.

According to Dangerous Substances and Explosive Atmosphere Regulations (DSEAR), a concentration of dissolved methane as low as 1.4 mg/L in leachate is known to be capable of giving rise to explosive methane levels in atmospheres in contact with it. A level of 0.14 mg/L is therefore considered to be a maximum safe amount of dissolved methane. [ENVIROS, 2009] All but one of the peat samples have concentrations higher than the safe amount for the leachate. The only sample where dissolved methane was not detected is the recently defrosted block of *Sphagnum* from Maine, which also shows least change of gas content determined by means of Ground Penetrating Radar (GPR) antennas.

In addition to the water chemistry test, conductivity and total dissolved solids (TDS) measurements were performed over entire duration of the experiment. All results show similar trends, however only the results for the WCA1 and *Sphagnum* (GLAP) samples are shown in Figure 4.23 for brevity. For each sample, water conductivity mimics almost exactly the trend of total dissolved solids, indicating that periods of higher conductivity coincide with more dissolved solids and vice versa.

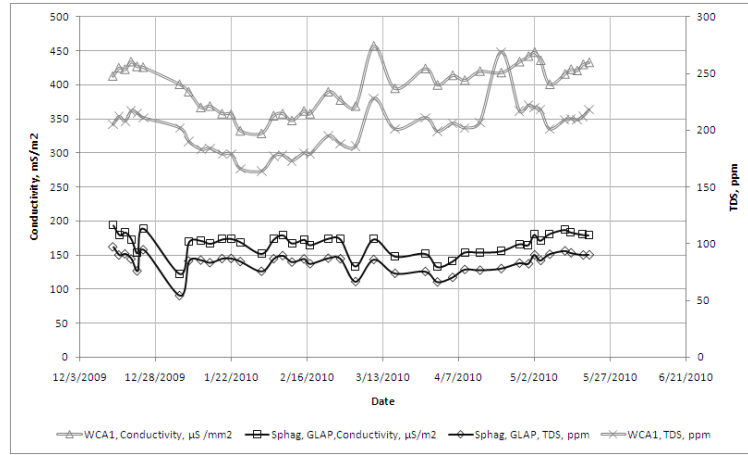


Figure 4.23: TDS and Conductivity measurements of WCA1 and *Sphagnum* (GLAP)

4.5 Porosity Test

Since the CRIM model requires values of porosity, we conducted measurements in laboratory for each sample (Chapter 2.3.5). Knowing the density of water ($\rho = 1g/cm^3$) we can easily calculate the volume of the saturated water (Table 4.12), which assumes full saturation equals to the porosity.

Sample	V_{total}, cm^3	M_{p+w}, cm^3	M_p, g	V_{Water}, cm^3	Porosity, %
WCA1	234.76	241.2	21.85	219.35	93.4
WCA1	234.76	251.1	40.20	210.90	89.8
WCA2	81.00	86.6	6.70	79.90	98.6
WCA2	129.85	121.8	11.40	110.40	85.2
<i>Sph</i> , GLAP	234.76	229.5	15.50	214.00	91.2
<i>Sph</i> , Maine	234.76	248.7	22.25	226.45	96.4
<i>Sph</i> , Maine	234.76	244.2	28.75	215.45	91.8

Table 4.12: Porosity Calculation: Total extracted volume and its mass, mass of dry peat and volume of water for each sample

The porosity measurements possibly carry the largest error due to the nature of the experiment. Theoretically, one has to extract a known volume of peat without disturbing the matrix and fully saturate it with water. In reality, extraction of the fixed volume of peat is rather challenging and does alter the peat matrix. However, regardless of all challenges, the results for all samples are well within the range of porosity values for peat soils (80% to 95% [Boetler, 1969]).

4.6 Exponential parameter comparison, WCA1

The average gas content of three horizontal lines (Line 1, 2 and 3) for peat Sample from WCA1 were compared for three different α parameters: (1) $\alpha = 0.35$ [Kellner et al, 2005]; (2) $\alpha = 0.5$ suggested by Brovelli [Brovelli et al, 2008] and (3) $\alpha = 0.04 \cdot \phi + 0.47 = 0.507$ for porosity $\phi = 91.6\%$. Brovelli et al, 2008] Figure 4.24 shows three curves for each choice of α .

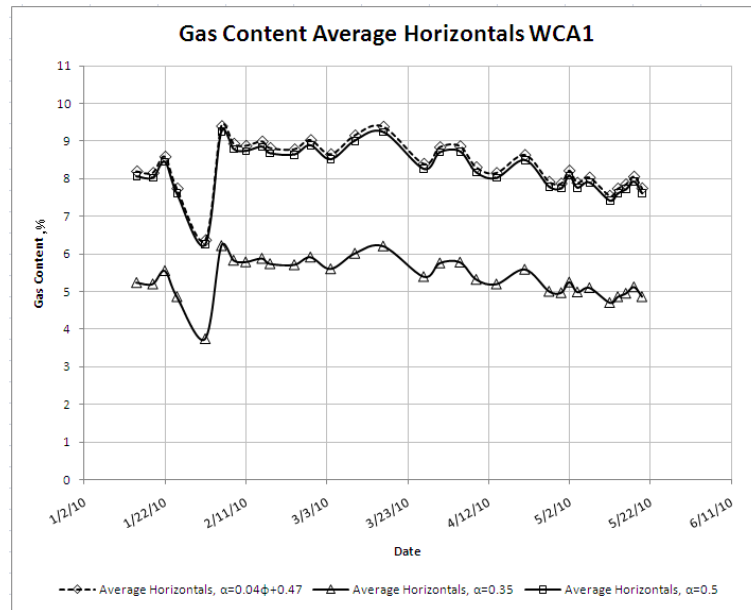


Figure 4.24: WCA1 gas content curves comparison depending on α

Also, the maximum change of gas content n was compared (Table 4.13) for all WCA1

lines.

LINE	$n, \% \alpha = 0.35$	$n, \% \alpha = 0.5$	$n, \% \alpha = 0.507$
Line 1	2.12	2.56	2.58
Line 2	2.44	2.94	2.97
Line 3	3.18	3.83	3.86
Line A	3.16	3.81	3.83
Line B	2.77	3.35	3.38
Line C	1.83	2.20	2.22

Table 4.13: Maximum change of gas content n for different parameters α

As expected, α parameter influences the gas content n estimations greatly (difference between $\alpha = 0.35$ and $\alpha = 0.5$ is $5.5 \% - 8.5 \% = 3 \%$), however the overall gas variability followed the same pattern and the gas change percentage does not depend on α in the same degree (max change for $\alpha = 0.35$ is 2.12% and for $\alpha = 0.5$ it is 2.56%). Consequently, since the main interest of this study is to investigate biogenic gas changes and ebullition mechanisms over time, using $\alpha = 0.35$ seems reasonable. Furthermore, previous studies have also shown further justification for using such values for Sphagnum peat soils [i.e. Comas et al, 2008; Parsekian et al, 2010].

4.7 Error calculations

Due to complexity of the CRIM equation (Eq. 2.12) the cumulative error propagation formula was used (Eqs. 4.7 and 4.8, where x is one parameter and total error Δn is estimated including all parameter that carry in an error). Two errors were calculated: (1) total amount of gas in the sample, δ_n , which is affected not only by variations of parameters like porosity variations due to surface deformation, but also overall approximations of constants, like soil relative dielectric permittivity ϵ_s , porosity ϕ etc.; and (2) gas change or volume of ebullition,

$\delta n_{\Delta n}$, which is smaller than δn due to the fact that once established constants, like ϵ_s , do not change in time ($\Delta n = n_2 - n_1$).

$$n + \Delta n_x = n(x + \Delta x) \quad (4.7)$$

$$(\Delta n)^2 = \sum (\Delta n_x)^2 \quad (4.8)$$

Table 4.14 lists percent errors of all the variables x in the equation 4.8 for total gas volume error calculations: (a) the porosity measurement carries in an error due to the nature of the experiment (approximated using three measurement for each sample); (b) the relative dielectric permittivity of water depends on the temperature as shown in figure 2.2, thus error associated with the fitting line is estimated to be approximately 0.5% [Buchner et al, 1999]; (c) the variance of bulk permittivity was calculated using the equation 4.9 and assuming that no error is carried in by time picking ($dt = 0$); (d) relative dielectric permittivity of soil approximation.

$$\frac{d\epsilon_b}{\epsilon_b} = 2 \cdot \frac{dv}{v} = 2 \cdot \frac{d(D)}{D} \quad (4.9)$$

where v is velocity of the signal and D is distance the signal travels.

Variable	σ	explanation
ϕ	$\pm 4\%$	deviation of three distinct measurements
ϵ_w	$\pm 0.5\%$	best fit line (fitting error)
α	0	assuming that is constant and does not change due to external factors
ϵ_b	$\pm 3.0\%$	due to velocity estimation (Eq. 4.9)
v	$\pm 1.5\%$	due to the sample holder deformation by the force exerted by peat on the sample holder's walls
D	$\pm 1.5\%$	deformation of the walls
ϵ_r	$\pm 20\%$	

Table 4.14: Measurements Variance for gas content error estimations

Table 4.15 lists percent errors of all the variables x in the equation 4.8 for volume of ebullition error estimation: (a) the porosity of the sample can change over time depending on the atmospheric pressure. The surface deformation measurement allowed us to account for porosity variations using equation: $\frac{n}{n_0} = \frac{L_0}{L}$, thus is as precise as surface deformation measurement; (b), (c) the same as for δn ; (d) once established, dielectric permittivity of soil is constant throughout the experiment.

Variable	σ	explanation
ϕ	$\pm 0.5\%$	due to pressure change estimated using surface deformation measurements ($\frac{n}{n_0} = \frac{L_0}{L}$, where L is height of the peat block)
ϵ_w	$\pm 0.5\%$	best fit line (fitting error)
α	0	assuming that is constant and does not change due to external factors
ϵ_b	$\pm 3.0\%$	due to velocity estimation (Eq. 4.9)
v	$\pm 1.5\%$	due to the sample holder deformation by the force exerted by peat on the sample holder's walls
D	$\pm 1.5\%$	deformation of the walls

Table 4.15: Measurements Variance for gas change error estimations

As expected, error for the total amount of gas for all sample was established to be 43% (Table 4.16 shows average values of fractional volumes of biogenic gas within each sample together with an average error) and average error for the gas change estimations is approximately 10% (Table 4.17). Given the nature of the CRIM model, the high percent error in the gas content estimate is mostly a result of the measured error in porosity. Such error estimate is based on porosity measurements at 3 locations along the sample and therefore neglects natural heterogeneity of the peat matrix. For that reason having an accurate measure of sample porosity will be critical in order to minimize the error associated with gas content estimates in future measurements.

Samples	$n \pm \delta n$
WCA1	4.63 ± 2.00
WCA2	5.93 ± 2.55
<i>Sphagnum</i> (GLAP)	5.04 ± 2.17
<i>Sphagnum</i> (ME)	6.20 ± 2.67

Table 4.16: Total gas volume measurement error

Samples	$n \pm \delta n_{\Delta n}$
WCA1	4.63 ± 0.46
WCA2	5.93 ± 0.59
<i>Sphagnum</i> (GLAP)	5.04 ± 0.50
<i>Sphagnum</i> (ME)	6.20 ± 0.62

Table 4.17: Gas change measurement error

5 Discussion

5.1 Gas content and ebullition fluxes

Average gas contents in this study range between 4.1% and 6.9% for both WCA1 and WCA2 samples and 3.7% and 7.9% for both *Sphagnum* samples. Such percents are well within range of estimated volumes of biogenic gases in peatlands as established between 0% and 19% of the peat volume in several other studies [Rosenberry et al., 2006]. The results for the emission rates in this study are also very consistent with other studies and are in the range of 0.08% and 0.4% gas content per day for Everglades samples and 0.01% and 0.41% per day for *Sphagnum* samples.

Given the contrasting latitudes between the peat soil samples shown in this study (i.e. boreal versus subtropical systems), the similarities in biogenic gas dynamics for all of the samples are quite striking, particularly in terms of biogenic gas buildup and release (Figures 4.13 and 4.14). The observed trend of gradual gas buildup in the two *Sphagnum* samples in the first few days of the experiment may be due to the fact that the experiment started right after these samples were defrosted, thus not giving them enough time to stabilize. Similar effects have been shown in previous laboratory studies involving defrosted peat blocks [i.e. Comas and Slater, 2007; Slater et al., 2007 and Strack et al., 2005].

Summing up all the gas volumes that each peat sample has emitted within the total 124 days length of the experiment, we can estimate the overall amount of produced gas as follows (with respect to the total volume 14.5L): WCA1 produced 22.3% (Line A - 7.6%, Line B - 9.2%, Line C - 5.5%); WCA2 produced 19.9% (Line A - 8.4%, Line B - 6.3%, Line C - 5.2%) and within 54 days *Sphagnum* (GLAP) produced 7.4% (Line A - 2.7%,

Line B - 2.3%, Line C - 2.5%) and *Sphagnum* (ME) produced 7.8% (Line A - 2.6%, Line B - 2.1%, Line C - 3.1%). Knowing that the total volume of sample holder is approximately 14.5L, the volume of gas produced by each sample is respectively 3.2L for WCA1, 2.9L for WCA2, 1.1L for *Sphagnum* (GLAP) and 1.14L for *Sphagnum* (ME). Assuming as in previous chapter that 54.0% of biogenic gas volume is methane [Glaser et al., 2004], and that 7% is carbon dioxide [Chanton et al., 1988], we can now use ideal gas law (Eq. 4.2) to estimate the total mass of the emitted over entire experiment gas and calculate the rate of emission, assuming direct effect of atmospheric pressure on gas volume is negligible (less than 1%).

The resulting average rates of CH_4 and CO_2 are presented in table 5.1 and are calculated by dividing total emissions during 124 days for Florida samples and 54 days for northern samples (columns 2 and 4) by the number of days (for sample calculation see eq. 4.4). The results are well within range of other studies performed in laboratory, which are 0 - 1,200 $mg \cdot m^{-2} \cdot d^{-1}$ [Baird et al., 2004; Christensen et al., 2003; Comas and Slater, 2007]; or in the field ranging between 48 and 35,000 $mg \cdot m^{-2} \cdot d^{-1}$ [Glaser et al., 2004; Tokida et al., 2007].

Gas emission (E_{CH_4}) is calculated summing all emitted gas of three vertical lines within the whole duration of the experiment, using equation 4.2 to estimate mass of methane and carbon dioxide and dividing it by the number of days (124 for Florida Samples and 54 for northern peatlands sample). An example of calculations of methane gas emission per surface area for WCA1 is shown in previous chapter (Equation 4.4) and the average emission rate is $E_{CH_4}/days = 17,530/124 = 141mg \cdot m^{-2}d^{-1}$

Table 5.1 shows overall emissions of methane (the second column) and carbon dioxide (forth column) per surface area over 124 days for WCA1 and WCA2 and 54 days for *Sphagnum* (GLAP) and *Sphagnum* (Maine). In addition, emission rates per day are calculated by dividing total emission by number of days and demonstrated for each sample in columns three and five.

Sample	Emission CH_4 , $mg \cdot m^{-2}$	Emission rate CH_4 , $mg \cdot m^{-2}d^{-1}$	Emission CO_2 , $mg \cdot m^{-2}$	Emission rate CO_2 , $mg \cdot m^{-2}d^{-1}$
WCA1	17,530	141	6,260	50
WCA2	15,670	126	5,590	45
<i>Sphagnum</i> (GLAP)	5,850	109	2,090	39
<i>Sphagnum</i> (ME)	6,180	114	2,200	41

Table 5.1: Gas Emissions per Surface Area and Average Rates of Methane and Carbon Dioxide Emission

Finally, average ebullition fluxes were calculated for each ebullition event (Table 4.9, where flux rate units are $mg \cdot C/m^2$ per day calculated using equations 4.5 and 4.6). Table 5.2 shows average of four ebullition rates (Table 4.9) of CH_4 and CO_2 separately along with the sum of both. We see again, that these rates are comparable with one another for all four samples.

Sample	Emission rate CH_4 , $mgC \cdot m^{-2}d^{-1}$	Emission CO_2 , $mgC \cdot m^{-2} \cdot d^{-1}$	Emission rate CH_4+CO_2 , $mg \cdot m^{-2}d^{-1}$
WCA1	118.35	15.36	133.68
WCA2	166.23	21.51	187.71
<i>Sphagnum</i> (GLAP)	146.13	18.93	165.06
<i>Sphagnum</i> (ME)	55.80	7.23	63.03

Table 5.2: Average CH_4 , CO_2 gas emissions of four single ebullition events per surface area per day for each sample.

5.2 Dynamics of ebullition

Given the episodic nature of gas content releases in all samples, ebullitive fluxes are recalled. Other studies (particularly at the field scale) have shown releases of methane with total volumes per square meter up to 10 times [i.e. Rosenberry et al. 2003] those reflected here, and reaching 30 times [i.e. Glase et al., 2004] in some areas. However, given the nature of current conceptual models for gas accumulation in peatlands (i.e. deep vs shallow gas model, see section 1.2.2 for details) it seems logical that limitations in gas entrapment for shallow peat soils will most likely result in smaller fluxes that are overall more repeatable over time. Furthermore, large releases of gas trapped under confining layers in the field are harder to detect due to their episodic nature. For instance, previous field studies in northern peatlands have detected volumes reaching up to $172,000 \text{ mgCH}_4/\text{m}^2$ during single ebullition events [i.e. Comas et al, 2008; Glaser et al. 2004]. The samples shown in this study, exemplify smaller scale ebullition events that are more periodical. These events seem to be very consistent no matter what the origin of the peat sample is. In this sense, it seems logical that such small scale ebullition events will be much more pronounced in samples from subtropical systems (i.e. Everglades) that maintain fairly constant temperatures throughout the year, versus boreal systems that often stay up to 4-5 months frozen (and thus almost inactive in terms of methanogenesis).

Although I understand the limitations of using this approach, particularly considering the heterogeneous nature of peat soils and that the ebullition fluxes represent an average flux value for each individual peatland, average emission rates can be measured for each peatland. For instance if we assume that the total area of both WCA is 861,440 acres ($3.5 \cdot 10^9 \text{ m}^2$) [Abtew et al., 2004], the rate of the methane and carbon dioxide production would be $0.47 \cdot 10^9$ grams per day and $0.17 \cdot 10^9$ grams per day respectively. Even though the *Sphagnum* samples were defrosted and the estimations of the total volume of emitted gas had to account for the stabilization time after the defrost, we see that the rates of gas

production for Everglades peat are higher than those of northern peatlands. Two possible reasons for that is the (1) *Sphagnum* samples were defrosted, thus stabilization time had to be accounted for in the gas emission rate calculations, (2) the experimental scale is small and cannot account for the total area of peatland gas production, and its related heterogeneity. In this sense it is possible to assume that the Everglades samples may be more efficient in terms of methane production under the room temperature conditions used during the experiment.

Furthermore, the *Sphagnum* from Maine was investigated for the least amount of days and the difference between the first day and second day shows an unusual increase in GPR gas content of over 5% for horizontal lines. In addition, the sample also shows an unusual drop in gas content after gas-meter measurements were initiated. A potential reason for such drop could be related to the extraction of the gas volumes along the edges of the sample, resulting in decrease of gas content along the horizontal survey lines 1, 2 and 3. Since gas bubbles were extracted along the vertical sides of the sample holder, it seems reasonable to expect such drop for those line measurements that cross that side (i.e. all traces perpendicular to the side), while vertical lines (crossing such sides only along one or two traces) would not be affected.

5.3 Effect of atmospheric pressure and correlation analysis

Traditionally, most studies have suggested that falling atmospheric pressure may induce gas ebullition events [Moore and Roulet, 1993; Fechner-Levy and Hemond, 1996; Rosenberry et al., 2003; Glaser et al., 2004; Kellner et al., 2004; 2005; Strack et al., 2005; Tokida et al., 2005]. However, it has also been suggested that as atmospheric pressure increases, the size of the gas bubble decreases making them more mobile and allowing bubbles to escape through the matrix pore space [Chanton and Martens, 1988; Beckwith and Baird, 2001]. The data shown in this thesis is overall very consistent with previous investigations on gas triggering mechanisms and dynamics in peat soils and suggest that ebullition events

are related to periods of atmospheric pressure increase. Data correlation analysis has been done in attempt to support this theory.

Considering that the direct gas volume change due to increased pressure cannot account for the entire volumetric change of gas content (less than 1% pressure change over entire experiment results in same percentage of volume change and can account only for less than 40% of the entire volume change, meaning gas emission accounts for more than 60% of volume change), four plots of atmospheric change versus volumetric gas change were generated (Figures 5.1, 5.2, 5.3, 5.4).

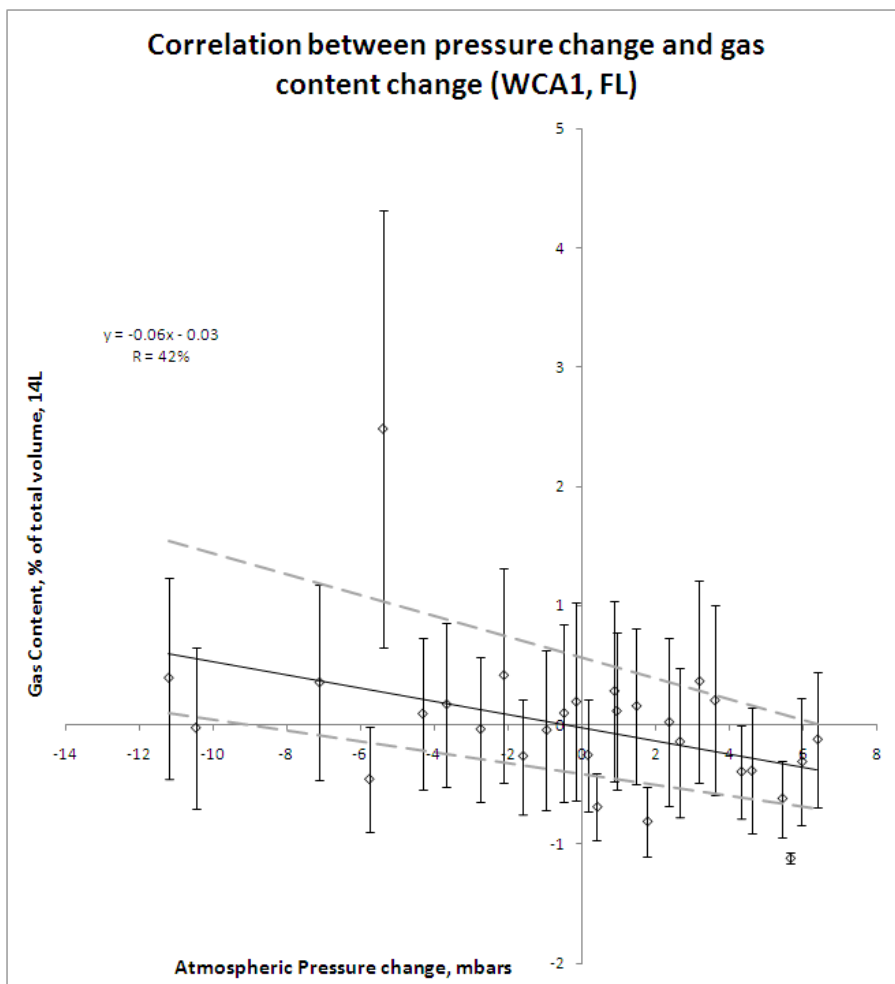


Figure 5.1: Atmospheric pressure change vs gas content change within WCA1 sample (dotted lines represent the best fit error)

Figure 5.1 shows a trend of negative atmospheric pressure change (decrease) generally corresponds to periods of positive $\frac{mR}{M}$ change (increase or gas accumulation) and vice versa. The correlation coefficient for these measurements is 43% and most of the datapoints follow this tendency within their error. In addition, the dotted lines represent error of the linear regression, however, any best fit line will have a negative slope, thus will still represent the trend. An estimated relation between gas change, ΔV , and atmospheric pressure, ΔP , change is shown below (Eq. 5.1).

$$\Delta V = (-0.06 \pm 0.01)\Delta P + (0.03 \pm 0.63) \quad (5.1)$$

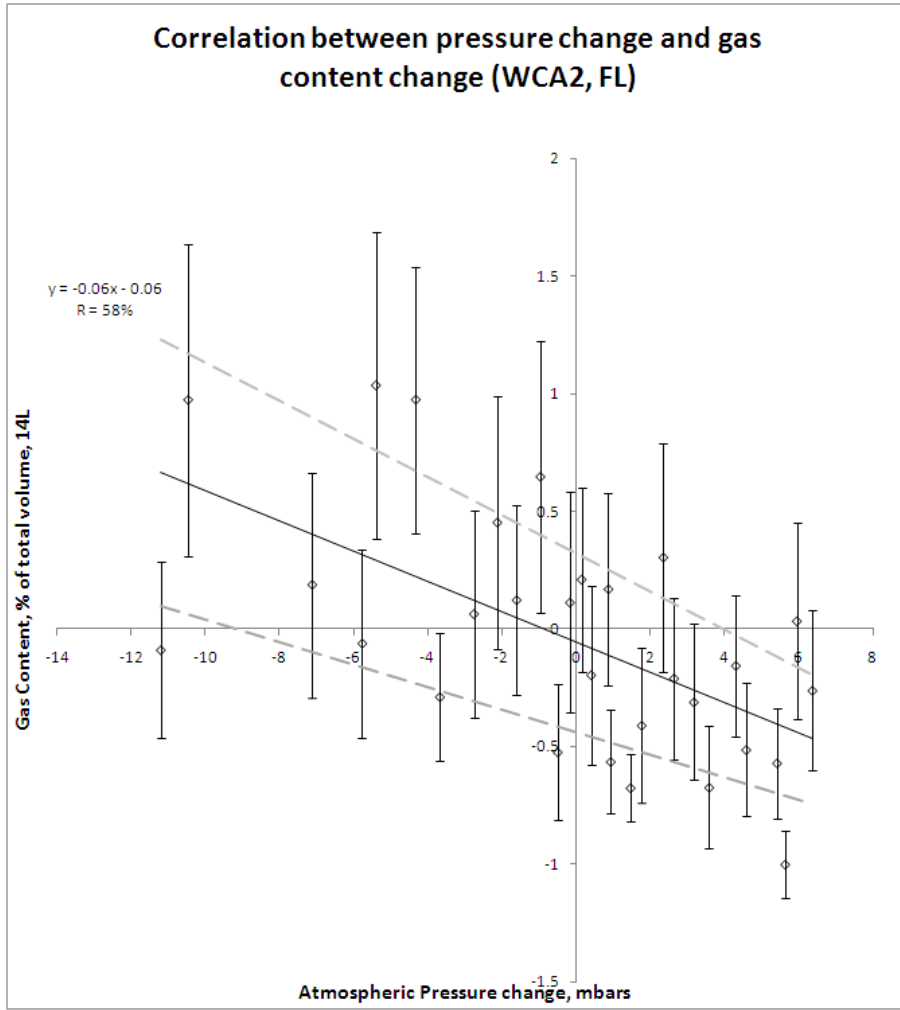


Figure 5.2: Atmospheric pressure change vs gas content change within WCA2 sample (dotted lines represent the best fit error)

Figure 5.2 demonstrates the same correspondence of atmospheric pressure increase with gas ebullitions, however correlation coefficient for these measurements is slightly higher - 57%. Also, similarly to WCA1 slope of the linear regression does not change signs within the error. As a result, the relation between ΔV and ΔP is the following (Eq. 5.2)

$$\Delta V = (-0.06 \pm 0.02)\Delta P + (0.06 \pm 0.38) \quad (5.2)$$

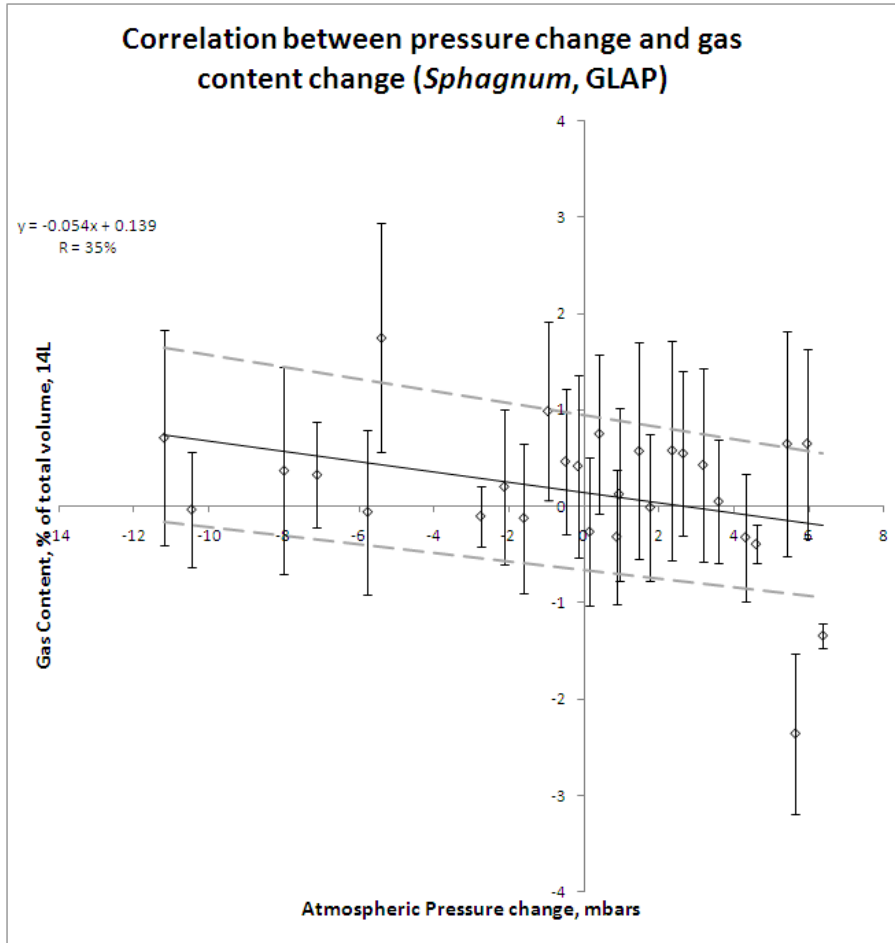


Figure 5.3: Atmospheric pressure change vs gas content change within *Sphagnum*, GLAP sample (dotted lines represent the best fit error)

Sphagnum, GLAP, measurements have the least correlation coefficient (35%). Above that, a slope can change from negative to positive within the error (Figure 5.3). This may indicate that *Sphagnum* peat is less effected by changes in atmospheric pressure that sub-tropical peats (Eq. 5.3).

$$\Delta V = (-0.05 \pm 0.09)\Delta P + (0.14 \pm 0.63) \quad (5.3)$$

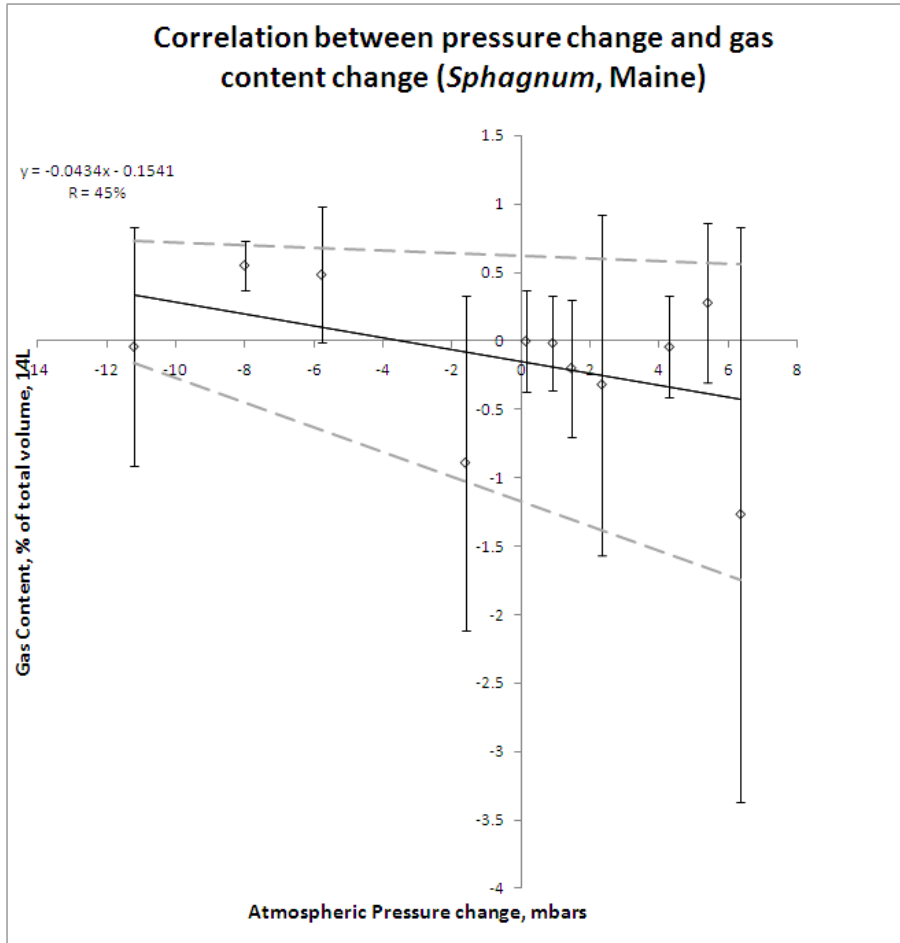


Figure 5.4: Atmospheric pressure change vs gas content change within *Sphagnum*, ME sample (dotted lines represent the best fit error)

Due to relatively small duration of the experiment for *Sphagnum* sample from Maine, less data of gas change is available, however even this limited amount of measurement produce the same trend as previous 3 samples (Figure 5.4) with correlation coefficient of 45%. Similarly to *Sphagnum* (GLAP) sample, the slope within the error can be positive or negative (Eq. 5.4).

$$\Delta V = (-0.04 \pm 0.08)\Delta P + (0.15 \pm 0.73) \quad (5.4)$$

For all four samples correlation coefficients were calculated using equation 5.5, where

x corresponds to pressure change and y corresponds to mass change, and is approximately 45% for every sample (43% for WCA1, 57% for WCA2, 35% for *Sphagnum* (GLAP) and 45% for *Sphagnum*, (ME)). The fact that both *Sphagnum* samples' correlation coefficients are smaller than Florida sample, might indicate that *Sphagnum* peat experience more complicated relation between changes of atmospheric pressure and gas content. In addition, for both Florida samples the slope of the regression is always negative, whereas for northern samples it is not fixed due to error of measurements, which can be an indicator, that there is an internal parameter that was not accounted in current experiment and which influences the gas production and ebullition.

$$r = \frac{n \sum(xy) - \sum(x) \sum(y)}{\sqrt{[n \sum x^2 - (\sum x)^2] [n \sum y^2 - (\sum y)^2]}} \quad (5.5)$$

The errors and correlation coefficients found here are such that it is hard to draw a firm conclusion. Furthermore, the experiment was not excluded from other than atmospheric pressure influences, internal and external. Nevertheless, the results do not contradict that in general increases of atmospheric pressure coincide with ebullition events, however more parameters are needed to be included in order for better correlation.

6 Future Work

For testing purposes, tomography was performed on Line 2 of sample WCA1 during April 3rd using a 2 cm separation. Preliminary results are shown in figure 6.1. The model itself has a limited resolution; however, we can distinguish areas of low permittivity (or high velocity) that could potentially represent a gas build-up areas or bubbles within the plane.

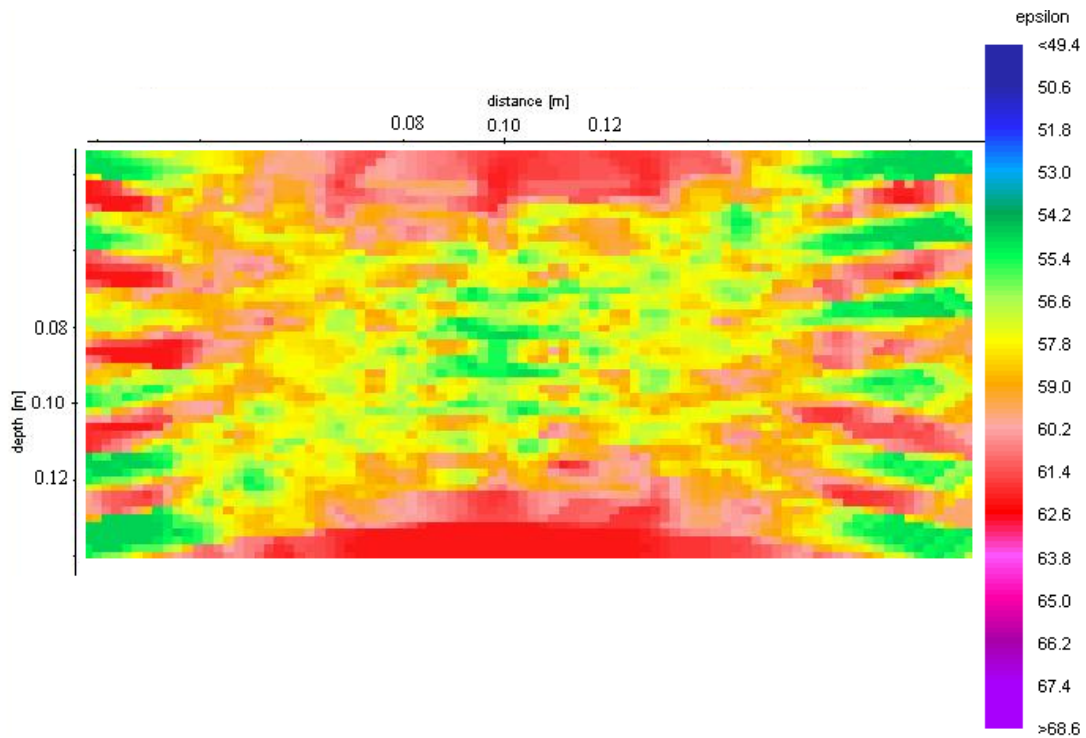


Figure 6.1: Tomography, WCA1, 2D velocity model

Figure 6.1 shows the results of 7 files processed out of 11 total collected. The original model of rays included 11 files (depth from 0 to 20 cm with 2 cm separation) (Figure 6.2),

where each ray represents one velocity measurement of the signal traveling from transmitter to receiver.

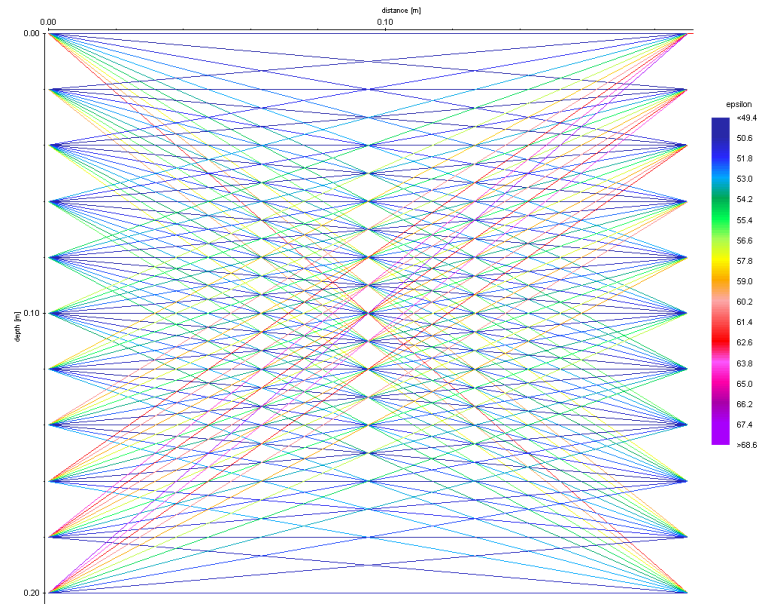


Figure 6.2: Original Tomography-Ray model (one ray represent EM signal traveling from Tx to Rx)

After several travel times for particular ray paths (i.e. the ones starting at 0.0 cm, 0.16 cm, 0.18 cm and 0.20cm on the transmitter) were removed due to unrealistically high velocities (up to 0.057 m/ns), the final model is depicted in Figure 6.4 and shows a maximum velocity 0.045 m/ns (well in the range of water saturated peat [Neal, 2004]).

Although these results are limited in terms of resolution they can be helpful for future considerations. The following error analysis was performed in order to enhance resolution of future models: it can be argued that in order for the model to be 100 % successful, the time change between two neighboring traces (Eq. 6.1)(Tx - Rx₁ and Tx - Rx₂ in Figure 6.3) has to be greater than the error of the velocity estimation $\Delta v/v$, due to the fact that velocities of the signal are computed for the final 2D model.

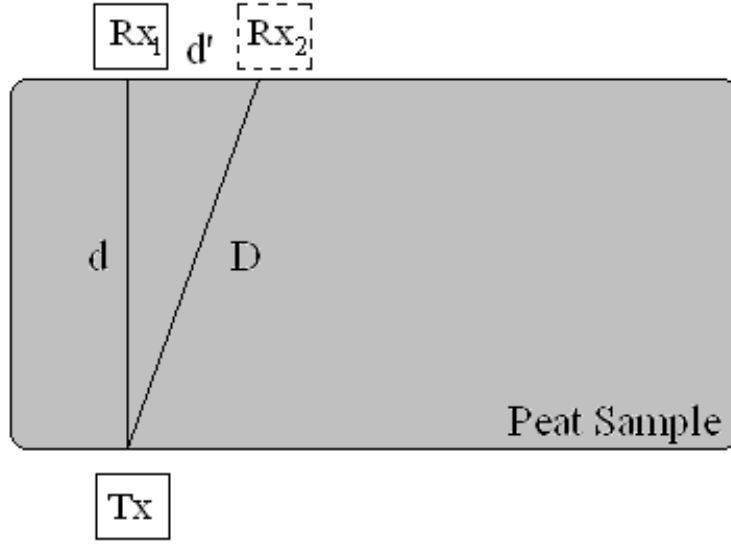


Figure 6.3: Two neighboring traces of Tomography profile

$$(T - t) = \frac{\Delta v}{v} \cdot t \quad (6.1)$$

That means that for this particular sample holder ($d=20\text{cm}$) and the percent error of $\Delta v = 2\%$ the minimum antenna separation d' can be estimated using equations 6.2 and 6.3, where v is the velocity of the signal and D is calculated from the Pythagoras' theorem ($D = \sqrt{d^2 + d'^2}$), assuming that EM wave does not deviate from a straight path (no diffraction):

$$\frac{\sqrt{d^2 + d'^2}}{v} = 0.02t + t = \frac{1.02d}{v} \quad (6.2)$$

The velocity of the signal cancels out and the minimum step d' for container width $d = 20\text{cm}$ can be calculated (Eq. 6.3).

$$d' = d\sqrt{(1.02)^2 - 1} \approx 20 \cdot 0.20 = 4.0(\text{cm}) \quad (6.3)$$

From this analysis it seems clear, that the dimensions of the investigated volume affect

the stability of the model and particularly its resolution ability. For that reason, limits have to be carefully considered when intending high resolution GPR tomography measurements in the lab. Future experiments should consider containers with bigger width to length ratio in order to be able to achieve better resolution.

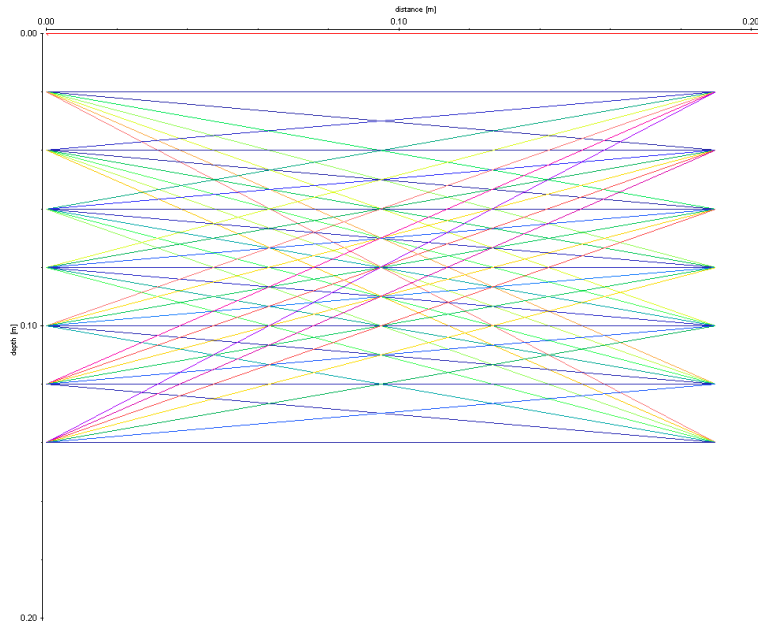


Figure 6.4: Final Tomography-Ray model

The following parameters were set to generate the 2D Line 2 image: space increment = 0.002, 2 rays were averaged (Average x = 2; average z = 2) and the velocity range was set 0.038 to 0.0405.

7 Conclusions

This study shows the potential of GPR measurements to non-invasively estimate and image the biogenic gas dynamics in peat soils using a unique instrumental setup in the laboratory. Several samples collected in both subtropical systems (i.e. Everglades) and northern peatlands (in Maine and Minnesota) showed strikingly similar trends in biogenic gas buildup and release, and total gas contents and emission fluxes consistent with previous laboratory studies of peat soils (i.e. rates of emissions are between $0.114 \text{ g} \cdot \text{m}^2 \cdot \text{d}^{-1}$ and $0.141 \text{ g} \cdot \text{m}^2 \cdot \text{d}^{-1}$ for methane and 0.039 to $0.050 \text{ g} \cdot \text{m}^2 \cdot \text{d}^{-1}$ for carbon dioxide). The data shown here suggests that rates of biogenic gas emissions for shallow peat soils in the Everglades may be similar or even higher than *Sphagnum* peat from northern peatlands. This effect may be enhanced by the fact that subtropical soils maintain temperatures more appropriate for CH_4 and CO_2 production throughout the entire year (as compared to boreal systems which may slow down such production during the winter time). Nevertheless, CH_4 and CO_2 production rates from Everglades peats are comparable to those from northern peatlands, hence showing the importance of emissions from subtropical peatlands in the global carbon cycle.

Furthermore, environmental variables, such as atmospheric pressure, showed mild correlation with biogenic gas dynamics for all samples measured. For instance, distinct events of atmospheric pressure increases coincide with decreases in gas content (i.e. changes in pressure as low as 10 mbar can trigger ebullition events of 0.4 - 0.5L of gas in 14.5 L peat blocks) within all peat samples suggesting that higher pressure may result in bubble size decrease and enhanced bubble mobility, as proposed by others. In addition, correlation

analysis between amount of atmospheric pressure increase and gas content drops within Florida and *Sphagnum* samples was presented, not contradicting the idea that higher pressure increases may be causing higher gas emissions.

Finally, 2D tomography was performed on all 4 samples, however only one measurement generated a realistic model. Although the results are only preliminary, the technique shows some potential for 2D imaging of gas distribution in peat soils.

Overall, this study presents a unique analysis of biogenic gas dynamics within peat samples of different latitudes and demonstrates similarities, as well as dissimilarities between northern and subtropical gas emissions and build up mechanisms. The results indicate that subtropical peatlands have to be further investigated in order to better constrain existing global gas dynamics and carbon cycling models.

8 Abbreviations

- CH_4 - Methane
- CO_2 - Carbon Dioxide
- COP - Common Offset Profile
- CRIM - Complex Refractive Index Model
- EM - electro-magnetic
- FPG - Free Phase Gas, gas in the free phase form (not dissolved in water)
- GLAP - Glacial Lake Agassiz Peatlands
- GPR - Ground Penetrating Radar
- HF - High Frequency
- LFG - Landfill Gas
- Porosity - relative volume of void space within a material
- Stack - (or stacking) single signal transmission (there are several stacks in one trace)
- Rx - Receiving GPR antenna
- TDR - Time Domain Reflectometry
- TDS - Total Dissolved Solids

- TRACE - composition of distorted and attenuated versions (as a result of the propagation medium) of the pulse emitted by the antennas [Rial et al., 2009]
- Tx - Transmitting GPR antenna
- WCA - Water Conservation Area
- ZOP - Zero Offset Profile

Bibliography

Abtew, W. , R. Scott Huebner and Violeta Ciuca, ”“Hydrology of the Everglades Protection Area””, *Everglades Consolidated Report, Ch.5*, 2004

Annan A.P., ”“Ground Penetrating Radar: Theory and Applications””, Chapter 1 ”“Introduction””, 2009

Ayalew, G., N.M. Holden and S.M. Ward, ”“Microwave dielectric properties of horticultural peat products””, *Mires and Peat*, VOL.2., ISSN 1819-754X, article 03, 2007

ASABE Standards, S358.2,AS 2008. S358.2. Moisture Measurement Forages. ASABE, St. Joseph, MI, 2008

ATSDR (Agency for Toxic Substances and Disease Registry), Arsenic, CASNo 7440-38-2, Division of Toxicology and Environmental Medicine ToxFAQ's, Atlanta, GA (USA), August 2007

Public Health Assessment, Final Release, Prepared by California Department of Public Health and Agency for Toxic Substances and Disease Registry (ATSDR), Atlanta, GA., 2010

Ayalew, G, N.M. Holden, S.M. Ward, ”“Microwave dielectric properties of horticultural peat products””, *Mires and Peat* VOL. 2, Art. 03, Int. Mire Cons. Gr. and Int. Peat Society, 2007

Baird, A.J., C.W. Beckwith, S. Waldron, J.M. Waddington, ”“Ebullition of methane containing gas bubbles from near-surface *Sphagnum* peat””, *Geophys. Res. Lett.*, 31,L21505, 2004

Beckwith CW, Baird AJ. 2001. Effect of biogenic gas bubbles on water flow through poorly decomposed blanket peat. *Water Resources Research* 37: 551558.

Blodau C, ”“Carbon cycling in peatlands A review of processes and controls””, 2002

Bottcher C J F, ”“Theory of Electric Polarisation””, Amsterdam:Elsevier, pp 415-420, 1952

Boelter,D.H. ”“Important Physical Properties of Peat Materials””, *Third International Peat Congress*, 1968.

Boelter, D.H, ”“Physical properties of peats as related to degreeof decomposition.””, *Soil Science Society of America Proceedings*,33, pp. 606609, 1969

- Brovelli A., Cassiani G., "Effective permittivity of porous media: a critical analysis of the complex refractive index model", *Geophysical prospecting*, 56, 715 - 727, 2008
- Randall B. Brown, Earl L. Stone, Victor W. Carlisle, "Ecosystems of Florida", USA, 1992, Chapter 3, pg. 35
- Buchner, R., J. Barthel and J. Stauber, "The dielectric relaxation of water between 0 C and 35 C" *Chem. Phys. Lett.* 306, pp 57-63, 1999
- Cameron, C.C., "Peat deposits of northeastern Pennsylvania", *U.S. Geological Survey Bulletin 1317 - A.*, pp. 90, 1970
- Chanton JP, Martens CS. 1988. Seasonal variations in ebullitive flux and carbon isotopic composition of methane in a tidal freshwater estuary. *Global Biogeochemical Cycles* 2: 289-298.
- Chadde, Steve W.; J. Stephen Shelly, Robert J. Bursik, Robert K. Moseley, Angela G. Evenden, Maria Mantas, Fred Rabe, Bonie Heidel, "Peatlands of National Forests of Northern Rocky Mountains: Ecology and Conservation", USA, 1998.
- Christensen T.R., N. Panikov, M. Mastepanov, A. Joabsson, A. Stewart, M. Oquist, M. Sommerkorn, S. Reynaud, B. Svensson, "Biotic controls on CO_2 and CH_4 exchange in wetlands - a closed environmental study", *Biogeochemistry*, 64, 337- 354, 2003
- Comas, X.; L. Slater 2007: "Evolution of biogenic gases in peat blocks inferred from noninvasive dielectric permittivity measurements" *WATER RESOURCES RESEARCH*, VOL. 43, W05424, doi:10.1029/2006WR005562
- Comas, X.; L. Slater, and A. Reeve, 2007: "In situ monitoring of free gas accumulation and release in peatlands using GPR", *Geophysical Research Letters* 34: L06402. 2007
- Comas, X., L. Slater, and A. Reeve, "Geophysical evidence for peat basin morphology and stratigraphic controls on vegetation observed in a northern peatland", *J. Hydrol.*, 295, 173-184, 2004
- Comas, X., L. Slater, "Non-invasive Field-scale Characterization of Gaseous-Phase Methane Dynamics in Peatlands Using GPR Method", *Carbon Cycling in Northern Peatlands, Geophysical monograph series 184*, American Geophys. Union, 2009
- Conyers, L.B.m "Ground-penetrating radar for anthropological research", *Antiquity*, Vol. 84, N323, pp. 175-184, 2010
- Coulthard, T.J, A.J. Baird, J. Ramirez, J.M. Waddington, "Methane Dynamics in Peat: Importance of Shallow Peats and a Novel Reduced-Complexity Approach for Modeling Ebullitions", *Carbon Cycling in Northern Peatlands, Geophysical Monograph Series 184*, pp. 173-185, 2009

- Glaser, P.H., J.P. Chanton, P. Morin, D.O. Rosenberry, D.I. Siegel, O. Ruud, L.I. Chasar, A.S. Reeve, "Surface deformation as indicators of deep ebullition fluxes in a large northern peatland", *Global Biochem. Cycles*, 18, GB1003, doi:10.1029/2003GB002069, 2004
- Craft, C.B., C.J. Richardson, "Soil Characteristics of Everglades Peatland", *The Everglades experiments: lessons for ecosystem restoration*, C.J. Richardson, New York, Springer 698, Ch. 3, 2008
- Daniels, M., T. Daniel, D. Carman, R. Morgan, J. Langston, K. VanDevender "Soil Phosphorus Levels: Concerns and Recommendations", University of Arkansas, Division of Agriculture, 1997
- Davis, R.B., Anderson, D.S. "A numeric method and supporting database for evaluation of Maine peatlands as candidate natural areas", *Maine Agricultural and Forest Experiment Station Technical Bulletin*, 175, 166 pp, 1999
- Dever, S.; Roberts, A. and Swarbrick, Dr. G., "Reducing the Greenhouse Impacts of Landfill Gas", Conference Paper for the NSW Waste Management Conference and Expo, September 2008. GHDSydney, NSW and Pells Sullivan Meynick, Sydney NSW, 2008
- Doolittle, J.A., J.R. Butnor "Soils, Peatlands, and Biomonitoring", *Ground Penetrating Radar: Theory and Applications* by J.H. Jol, Part II, Chap. 6, pp. 179 -192, 2009
- Enviros Methane stripping, DSEAR regulations, August 2009
- Ekono, "Report on energy use of peat", Contribution to U.N. Conference on the New and Renewable sources of Energy, Nairobi
- Fechner-Levy EJ, Hemond HF. 1996. Trapped methane volume and potential effects on methane ebullition in a northern peatland. *Limnology and Oceanography* 41: 1375-1383.
- Galland, P.E., "Methanogenic Archaea in boreal peatlands", Academic Dissertation in General Microbiology, General Microbiology, Department of Biological and Environmental Sciences, University of Helsinki
- Glaser, P.H., J.P. Chanton, P. Morin, D.O. Rossenberry, D.I. Siegel, O. Ruud, L.I. Chasar, A.S. Reeve, "Surface deform. as indicators of deep ebullitions fluxes in a large northern peatland", *Global Biochemisty Cycles*, 18 GB1003, doi:10.1029/2003GB002069, 2004
- Gleason, P.J., and Stone, Peter, 1994, Age, origin, and landscape evolution of the Everglades peatland, in Davis, S.M., and Ogden, J.C., eds., *Everglades- The ecosystem and its restoration*: Delray Beach, Fla., St. Lucie Press, p. 149-197.
- Goldstein J.H., "The impact of the Federal Programs on Wetlands: a report to congress by the Secretary of the interior" Vol II, Ch. 7, 1994.
- Mala Geosciences, "What is Radar", www.malags.com, GPR antenna manual.

Hales, B.A., C. Edwards, D.A. Ritchie, G. Hall, R.W. Pickup, J.R. Saunders, "Isolation and Identification of Methanogen-Specific DNA from Blanket Bog Peat by PCR Amplification and Sequence Analysis", *Applied and Environmental Microbiology*, 0099-2240/96/, pp. 678 - 675, 1996

Holden N.M. "The use of time domain reflectometry to measure water content of milled peat", *Irish Journal of Agricultural and Food research* 36, pp. 195-203, 1997.

Hooijer, A., M. Silvius, H. Woesten and S. Page, "Peat- CO₂: Assessment of CO₂ emissions from drained peatlands in SE Asia", *Delft Hydraulics report Q3943*, pp. 41, 2006

Hu, F.S. and R.B. Davis, "Postglacial development of a Maine bog and paleoenvironmental implications", *Botany, Can. J. Bot.* 73(4): 638649 (1995), doi:10.1139/b95-068, NRC Canada, 1995

IEEE "Standard 100 Dictionary of IEEE Standards Terms", Seventh Edition, *The Institute of Electrical and Electronics Engineering*, New York; ISBN 0-7381-2601-2; page 288, 2000

Iglesias, T.P., J.P. Fernandez, "A new approach for prediction of the permittivity of mixtures", *The Journal of Chemical Thermodynamics* Volume 33, Issue 10, pp. 1375-1381, 2001

Ineson, P., P.A. Coward, U.A. Hartwig, "Soil gas fluxes of N₂O, CH₄ and CO₂ beneath *Lolium perenne* under elevated CO₂: The Swiss free air carbon dioxide enrichment experiment", *Plant and Soil, Vol. 198*, doi:10.1023/A:1004298309606, 1998

IPCC, "Climate change": *The physical science basis, Contribution of working group I to the fourth assessment report of the intergovernmental panel on climate change*, S. Solomon, D. Qin, M. Manning, Z. Chen, M. Marquis, K. B. Averyt, M. Tignor, H. L. Miller and C. U. Press. Cambridge, UK and New York, USA: 996, 2007

Kellner E, Price JS, Waddington JM. 2004. Pressure variations in peat as a result of gas bubble dynamics. *Hydrological Processes* 18: 2599-2605

Kadlec, R.H., Scott Wallace, "Treatment Wetlands", Second Edition, NW USA, 2009

Kellner, E., J.M. Waddington, J.C. Price "Dynamics of biogenic gas bubbles in peat: potential effects on water storage and peat deformation", *Water Resour. Res.* 41, W08417, doi:10.1029/2004WR003732, 2005

Kellner, E, L.C. Lundin, "Calibration of Time Domain Reflectometry for Water Content in Peat Soil", *Nordic Hydrology* 32 (4/5), pp. 315-332, 2001

Kuntz, L.A., "Figuring Out Phosphates", *Articles pH*, USA, June 2006

Landtec GEMTM2000 gas analyzer & extraction monitor, operation manual, January 25, 2005, by CES-Landtec, CA, USA

Lee,D.B., "Effect of the eruption of Mount St. Helens on Physical, Chemical, and Biological Characteristics of Surface Water, Ground Water, and Precipitation in the Western United States", United States Geological Survey Water Supply Paper 2438, USA Government Printing Office, 1996.

Looyenga H, "Physica" 31, 401-406, 1965

Malmer, N., "Development of bog mires", *Coupling of land and water systems* by Hasler A.D., Springer-Verlag, New York, pp. 85-92, 1975

MALA Professional Explorer, The ProEx Control Unit, Operating Manual, Version 1.0

MALA Presentation, "What is Radar? Radio Detection and Ranging", Charleston, SC, USA

Martini, I.P., A. Martinez, W. Chesworth, "Peatlands: Evolution and Records of Environment and Climate Changes", CH. 7, edited by J.F. Shroder, Netherlands, 2006

Mastepano, M., C. Sigsgaard, E.J. Dlugokencky, S. Houweling, L. Strom, M.P. Tamstorf, T.R. Christensen, "Large tundra methane burst during onset of freezing", *Nature* 456, 628-630; doi:10.1038/nature07464, 2008

Matthews, E., "Wetlands", *Atmospheric Methane: Its Role in the Global Environment* (M.A.K. Khalil, ed.), pp. 202-233. Springer-Verlag, Berlin, 2000

Mitsch, W.J., James G. Gosselink, Christopher J. Anderson, Li Zhang, "Wetland Ecosystems", USA, 2009, pg. 3, pg. 160 - 189

Moore, P.D. and D.J. Bellamy, "Peatlands", Springer-Verlag, New York, pp. 221, 1974

Moore TR, Roulet NT. 1993. Methane flux: water table relations in northern wetlands. *Geophysical Research Letter* 20: 587590.

Neal, A., C.L. Roberts, "Applications of ground-penetrating radar (GPR) to sedimentological, geomorphological and geoarchaeological studies in coastal environments" In: Pye, K., Allen, J.R.L. (Eds.): *Coastal and Estuarine Environments: Sedimentology, Geomorphology and Geoarchaeology*, Geol. Soc.London Spec. Publ. 175, 139 171, 2000

Neal A., "Ground Penetrating Radar and its use in Sedimentology: principles, problems and progress", *Earth Science Review*, 2004

Nelson, S.O., "Measurement and calculation of powdered mixture permittivities", *IEEE Transaction on Instrumentation and Measurement*, Vol 50, No. 5, 2001

Novakov,T., T.W. Kirchstetter, J.E. Sinton, J.A. Sathaye (Environmental Energy Technologies Division), V. Ramanathan (Center of Atmospheric Sciences, Scripps Institute of Oceanography), J.E. Hansen, M. Sato (NASA Goddard Institute for Space Studies), "Large historical changes of fossil-fuel black carbon aerosols", USA, September 2002

- Osberg, P.H., Hussey II, A.M., Boone, G.M. "Bedrock geologic map of Maine", 1:500,000. *Maine Geological Survey*, 1985. Maine Department of Conservation.
- Parsekian, A.D., L. Slater, X.Comas, P.H. Glaser, "Variations in free-phase gases in peat landforms determined by ground-penetrating radar", *Journal of Geophysical Research*, VOL115, G02002, 2010
- Parsons, M.J., Nathaniel P. Saladin, David T. Long, Merideth L. Fitzpatrick, "Origin of Chloride in Wetlands Lakes, and Rivers of Michigan Lowlands", Michigan State University, Geological Society of America Abstracts with Programs, vol. 40, N. 6, pg. 346, October 2008.
- Patten, B.C., S.E. Jorgensen, "Complex Ecology: The Part-Whole Relation in Ecosystems", Prentice Hall, Englewood Cliffs, NJ, pp. 705, 1995
- Pihlatie, M.K., M. K. Pihlatie, R. Kiese, N. Brggemann, K. Butterbach-Bahl, A.-J. Kieloaho, T. Laurila, A. Lohila, I. Mammarella, K. Minkinen, T. Penttil, J. Schnborn, and T. Vesala, "Greenhouse gas fluxes in a drained peatland forest during spring frost-thaw event", *Biogeosciences*, 7, 1715-1727, 2010
- Price, J. S., "Role and characteristic of seasonal peat soil deformation on the hydrology of undisturbed and cutover peatlands", *Water Resour. Res.*, 39(9), 1241, doi:10.1029/2002WR001302, 2003
- Redman J.D., "Contaminant Mapping", *Ground Penetrating Radar* by H.J. Jol, Chap. 8, pp. 247 - 269, 2009
- Rial, F., M. Pereira, H. Lorenzo, P. Arias, A. Novo, "Vertical and Horizontal Resolution of GPR bow-tie Antennas" Natural Resources and Environmental Engineering, University of Vigo, Campus A Xunqueira s/n. 36005-Pontevedra, Spain, 2005
- Fernando I. Rial, Henrique Lorenzo, Manuel Pereira, Julia Armesto, "Waveform Analysis of UWB GPR Antennas", *Sensors* 2009, 9, 1454-1470; doi:10.3390/s90301454; ISSN 1424-8220
- Richardson, C.J., J.K. Huvane, "Ecological Status of the Everglades: Environmental and Human Factors that Control the Peatland Complex on the Landscape", *The Everglades Experiments Lessons for ecosystem restoration*, pp. 702, 2008
- Romanowitz E.A., Siegel D.I., Chanton J.P. Glaser P.H., "Temporal variations in dissolved methane deep in Lake Agassiz peatlands", Minnesota, *Global Biogeochemical Cycles* 9, pp. 197 - 212, 1995
- Rosenberry DO, Glaser PH, Siegel DI, Weeks EP. 2003. Use of hydraulic head to estimate volumetric gas content and ebullition flux in northern peatlands. *Water Resources Research* 39: 1066, DOI:10.1029/2002WR001377.

Rosenberry, D.O., P.H. Glaser, D.I. Siegel, "Hydrology of northern peatlands as affected by biogenic gas: current developments and research needs", *Hydrological Processes*, 20, 3601 - 3610, 2006

Sandmeier K.J, "ReflexW version 4.5.5", software manual, Germany, 1998.

Sharpley, A.N., T. C. Daniel and D. R. Edwards, "Phosphorus Movement in the Landscape," *J. Prod. Agric.*, Vol.6, No. 4, 1993.

Slater, L., X. Comas, D. Ntarlagiannis, M.R. Moulik "Resistivity-based monitoring of biogenic gases in peat soils" *WATER RESOURCES RESEARCH*, VOL. 43, W10430, doi:10.1029/2007WR006090, 2007

Strack M, Kellner E, Waddington J.M.. "Dynamics of biogenic gas bubbles in peat and their effects on peatland biogeochemistry", *Global Biogeochemical Cycles* 19: GB1003. DOI:10.1029/2004GB002330, 2005

Strack, M., T. Mierau, "Evaluating spatial variability of free-phase gas in peat using ground-penetrating radar and direct measurement" *JOURNAL OF GEOPHYSICAL RESEARCH*, VOL. 115, G02010 doi:10.1029/2009JG001045, 2010

Tarnocai, C., C.D.A. Rubec "Wetlands of Canada", Polyscience Publications Inc., Quebec, 1988

Tokida T., Miyazaki T., Mizoguchi M., "Ebullition of methane from peat with falling atm. pressure", *Geophys. Research Lett.*, 32: L13823, DOI:10.1029/2005GL022949, 2005

Tokida, T., T. Miyazaki, Mizoguchi, M. Nagata, O. Takakai, F.A. Kagemoto, R. Hatano, "Falling atm. pressure as a trigger for methane ebullition from peatland", *Global Biogeochem. cycles*, VOL. 21, GB2003, doi:10.1029/2006GB002790, 2007

Topp, G. C., J. L. Davis, and A. P. Annan, Electromagnetic determination of soil water content: Measurements in coaxial transmission lines, *Water Resour. Res.*, 16(3), 574-582,

Turunen, J., E. Tomppo, K. Tolonen and A. Reinikainen, "Estimating carbon accumulation rates of undrained mires in Finland - application to boreal and subarctic regions." *Holocene* 12: 69-80, 2002

D. Uduwawala, M. Norgren, P. Fuks "A complete FDTD simulation of a real GPR antenna system operating above lossy and dispersive grounds", *Progress in electromagnetic research*, PIER 50, 209-229, 2005

Whalen, S.C., "Biogeochemistry of Methane Exchange between Natural Wetlands and the Atmosphere", *Environmental Engineering Science*, Vol. 22, N1, Mary Ann Liebert, Inc, 2005

Williams, R., Crawford, R., "Methane Production in Minnesota Peatlands", *APPLIED AND ENVIRONMENTAL MICROBIOLOGY*, Vol. 6, pp. 1266-1271, 1984